NUCLEAR RELAXATION AND SPECIFIC HEAT STUDIES IN A STRONG ELECTRON–PHONON COUPLING SUPERCONDUCTOR HfV_2

Yutaka KISHIMOTO

Department of physics, Faculty of Engineering,
Tokushima University, Tokushima 770

December, 1990

Contents page

ABSTRACT

The Laves phase C15 compounds as well as A15 compounds have been known to exhibit the properties due to the strong electron–phonon coupling such as the fairly high temperature superconductivity, the saturation of the electric resistivity and the electronically induced lattice instability. Recently, a concept of two level system (TLS model) suggested that the anisotropy of their superconducting energy gap should be studied in connection with the heavy Fermions. In order to investigate whether the energy gap in HfV_2 is of the BCS type or not, the nuclear spin-lattice relaxation rates $1/T_1$ for ^{51}V and specific heat C have been measured.

The value of the electronic specific heat coefficient γ was estimated to be 47.7 mJ/mol·K^2. This value is about forty times as large as the value of 1.2 mJ/mol·K^2 for the typical superconductor Al with weak electron-phonon coupling , while this value is much smaller than γ=1000 mJ/mol·K^2 for the typical heavy Fermion superconductor $CeCu_2Si_2$. The electronic part of the specific heat is proportional to T^3 at low temperature, which is inconsistent with the BCS theory. These results suggest that the "slightly heavy electrons" take part in the superconductivity.

As for the spin-lattice relaxation rate, $1/T_1T$ is constant between 9.4 K and 20 K (T_c=9.2 K), decreases with increasing temperature, shows a small peak due to the martensitic phase transition near 110 K, and is nearly constant at temperatures T>130 K in the normal state. The temperature dependence of $1/T_1T$ between 20 K and 100 K was explained by using the narrow

band models with the half width of about 100 K.

In the superconducting state, $1/T_1$ shows a very small enhancement just below T_C and decreases rapidly with decreasing temperature. The $1/T_1$ is nearly proportional to T^5 well below T_C. It was found that the agreement between the data and the ABM curve with the gap parameter $\Delta/k_B T_C = 0.8 \times 2.014$ is satisfactorily good at low temperature. The frequency dependence of $1/T_1$ is weak and the small enhancement just below T_C is not affected by the external field at 12 MHz.

The field cycle method was also employed to measure T_1 in the zero field condition in the temperature range between 0.77 K and 4.2 K. The obtained $1/T_1$ data show the same T^5 dependence in this temperature range. The dependence of T_1 on the magnetic field in which the ^{51}V nuclear spins relax in the field cycle method was measured at 2.77 K. The T_1 is constant up to 100 Oe, be comes longer with increasing the field and again constant above 500 Oe. This field dependence is explained by the electric quadrupole effect.

These facts that the spin-lattice relaxation rate $1/T_1 \propto T^5$ well below T_C and the specific heat $C \propto T^3$ at low temperature indicate that the superconducting energy gap is anisotropic and vanishes at points on the Fermi surface. This gap anisotropy and the formation of the narrow sharp band in the normal state support the TLS model.

§1. Introduction

In fairly high *Tc* superconductors called strong electron-phonon coupling superconductors (abbreviated here after SCS), A 15 compounds , C 15 Laves phase compounds, Chevrel and rhodium boride compounds have the following anomalous properties [1]. 1) The electric resistivity in the normal state has a tendency to be saturated, approaching to the " Mott limit ", in which the mean free path becomes of atomic size. 2) The magnetic susceptibility and the Knight shift strongly depend on temperature . 3) The electronic specific heat coefficient γ is large. 4) The martensitic phase transitions are observed in some of these compounds.

The conventional theories have attributed these properties to the idea that the Fermi level acrosses a narrow band peak. The band calculations really show a sharp peak near the Fermi level. However, in 1983, Anderson and Yu[2] proposed a new viewpoint against the conventional treatment. The anomalies in these compounds are insensitive to the stoichiometry of the sample, although the change in the stoichiometry must shift the Fermi level. Therefore, the peak at Fermi level should be considered to be due to a many body effect. They regarded the strong electron-phonon coupling as the most important feature of these compounds. By treating the electron-phonon interaction as an interaction between the local phonon and the electron gas, Anderson and Yu found the ionic potential to be a type of double well, in which the lattice ions have two stable positions. These two configurations of the ionic state induce the structural phase

transition. This ionic system is called the two level system (TLS). Vladar and Zawadovsky[3] proved the interaction between a TLS and conduction electrons can be transformed to the $s-d$ interaction in the spin 1/2 impurity Kondo system. In the TLS model, these two ionic states play a role of the two degrees of freedom of the spin in the Kondo system. At low temperature the electron scattering by TLS at each lattice site becomes coherent, which is called the periodic TLS problem and just corresponds to the dense Kondo system.

Therefore, Matsuura and Miyake[4] regarded these strong electron-phonon coupling superconductors as a type of the heavy Fermion superconductors (HFS). This classification has another reason[5]. Several transition metals take a universal value, $A/\gamma^2 \fallingdotseq 0.4 \times 10^{-6}$ ($\mu\Omega$ cm$\cdot$ (mol$\cdot$K / mJ)^2), while the heavy Fermion compounds take another universal value $A/\gamma^2 = 1.0 \times 10^{-5}$, where γ is the electronic specific heat coefficient and A the proportionality constant of the electronic resistivity to T^2. The values of A/γ^2 for the typical SCS, Nb_3Sn and V_3Si are close to the latter value for HF compounds .

The HFS has the following characteristics[4] . 1) The interaction potential is q-dependent as it is composed of the onsite repulsion and the intersite attraction. 2) The retardation effect does not work since the heavy Fermion band width is smaller than the Debye frequency. Because of these characteristics, the non-s symmetry pairing becomes dominant and the superconducting energy gap becomes anisotropic and vanishes at points on the Fermi surface. In this case T^n-behavior for the electronic specific

heat, NMR relaxation rate $1 / T_1$ and the ultrasonic attenuation are expected at low temperature .

In order to inspect whether the above ideas are reasonable or not, it is very important to measure the physical quantities reflecting the properties of low energy electronic excitation spectrum such as nuclear spin-lattice relaxation rates and specific heat. In this paper we report the results of the specific heat and the relaxation rate $1/T_1$ for one of the SCS , HfV_2 .

§2. Experimantal Procedure

The sample of the polycrystal HfV_2 was prepared from stoichiometric starting materials , Hf of 99.9 % purity and V of 99.9 % purity , by Ar plasma-jet melting. The obtained button was turned over and remelted ten times to ensure the homogeneity . The ingot was annealed at 1000 ℃ in a vacuum for a week . The obtained sample was cut into a shape of 1x1x12 mm^3 for the specific heat measurement and crushed into the 200 mesh powder for the NMR measurement. The superconducting transition temperature T_c , which is defined as the mid point of transition , was determined to be 9.2 K by the ac susceptibility and the electronic resistivity measurements .

The specific heat was measured in the temperature range from 1.7 K to 18 K employing the conventional heat pulse method. The nuclear spin-lattice relaxation rate $1/T_1$ of ^{51}V nucleus was measured by using a conventional phase coherent pulsed spectrometer at 12 MHz in the temperature range from 0.8 K to 300 K . Below 4.2K the field cycle method[6] was employed in order to estimate T_1 precisely under the zero field condition. The measurement of T_1 at zero field is indispensable for the detection of the low energy electronic excitation because in the applied field T_1 below T_C becomes shorter by the spin diffusion to the vortex core.

§3. Specific heat

The measured specific heat C is shown in Fig. 1 (a) by plotting C/T versus T^2 in the temperature range from 1.7 K to 18 K. With decreasing temperature , C/T decreases monotonously and discontinuously increases at T_c = 9.2 K . This temperature 9.2K coincides with the critical temperature measured by electronic resistivity and ac susceptibility. Any other anomaly is not observed , which means our sample has no secondary phase and is sufficiently homogeneous.

These data above T_c can be fitted by the power series

$$C = \gamma T + \beta T^3 + \alpha T^5 + \delta T^7 . \qquad (1)$$

In order to determine these coefficients we considered the restriction that the entropy is continuous at T_C. The best fit coefficients are given in Table 1. Similar results are obtained by Luthi et al[7]. This value of γ = 47.7 mJ / mol · K^2 is about forty times as large as the values γ=0.8 mJ / mol · K^2 for free electrons or γ= 1.2 mJ / mol · K^2 for the typical weak electron-phonon coupling superconductor Al, but much smaller than γ=1000 mJ /mol · K^2 for the typical HFS $CeCu_2Si_2$[8] .

In general, γ and β are given by

$$\gamma = (2 / 3) \pi^2 k_B^2 N(E_F) (1 + \lambda), \qquad (2)$$

and

$$\beta = 12 \pi^4 k_B n / (5 \Theta_D^3), \qquad (3)$$

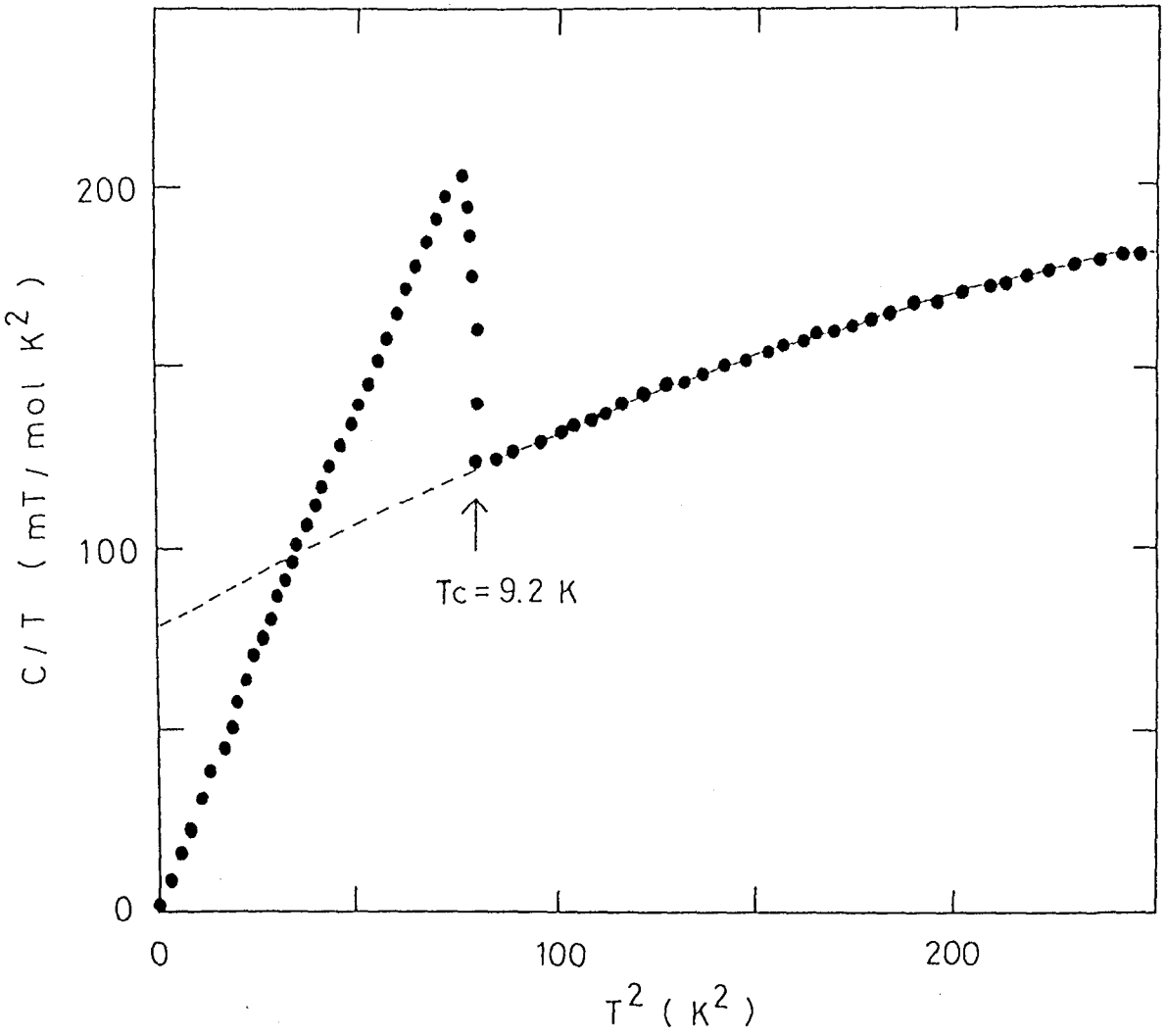

Fig. 1 (a) Specific heat C of HfV_2 in a plot C/T versus T^2. Dashed curve is an extrapolation of the higher T data to T=0.

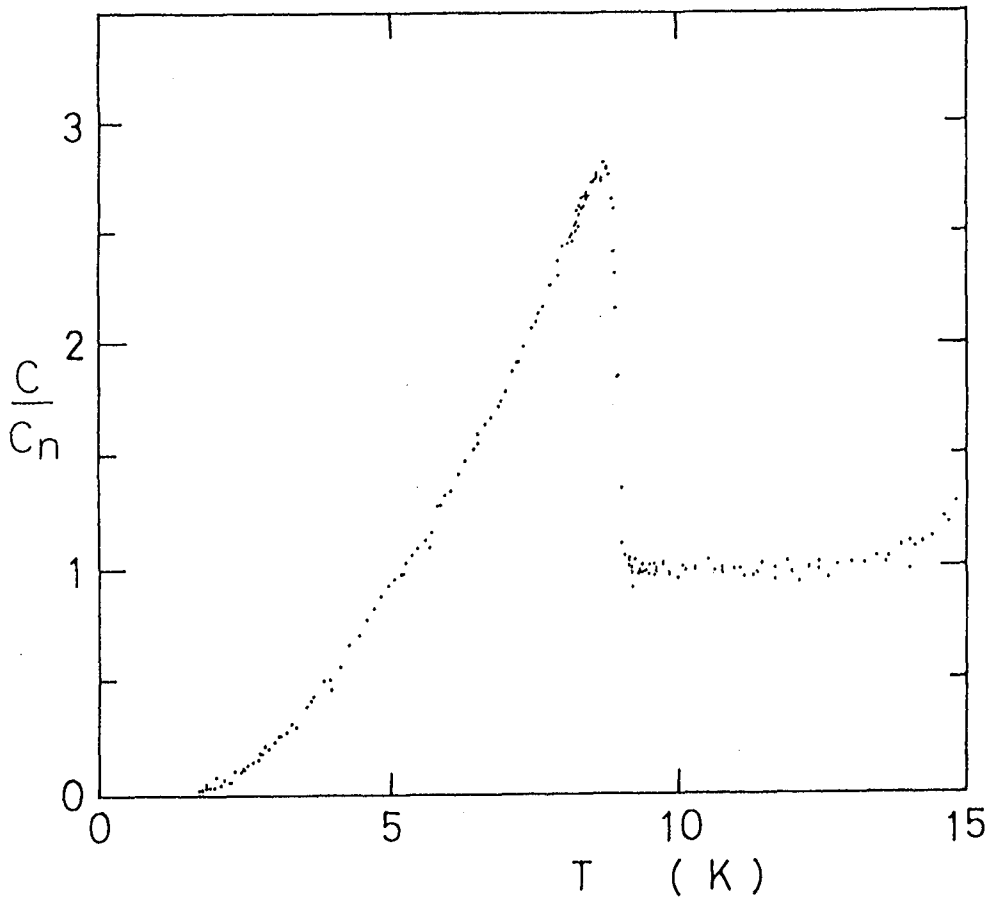

Fig. 1 (b) Eletronic specific heat data divided by γT_c plotted versus T.

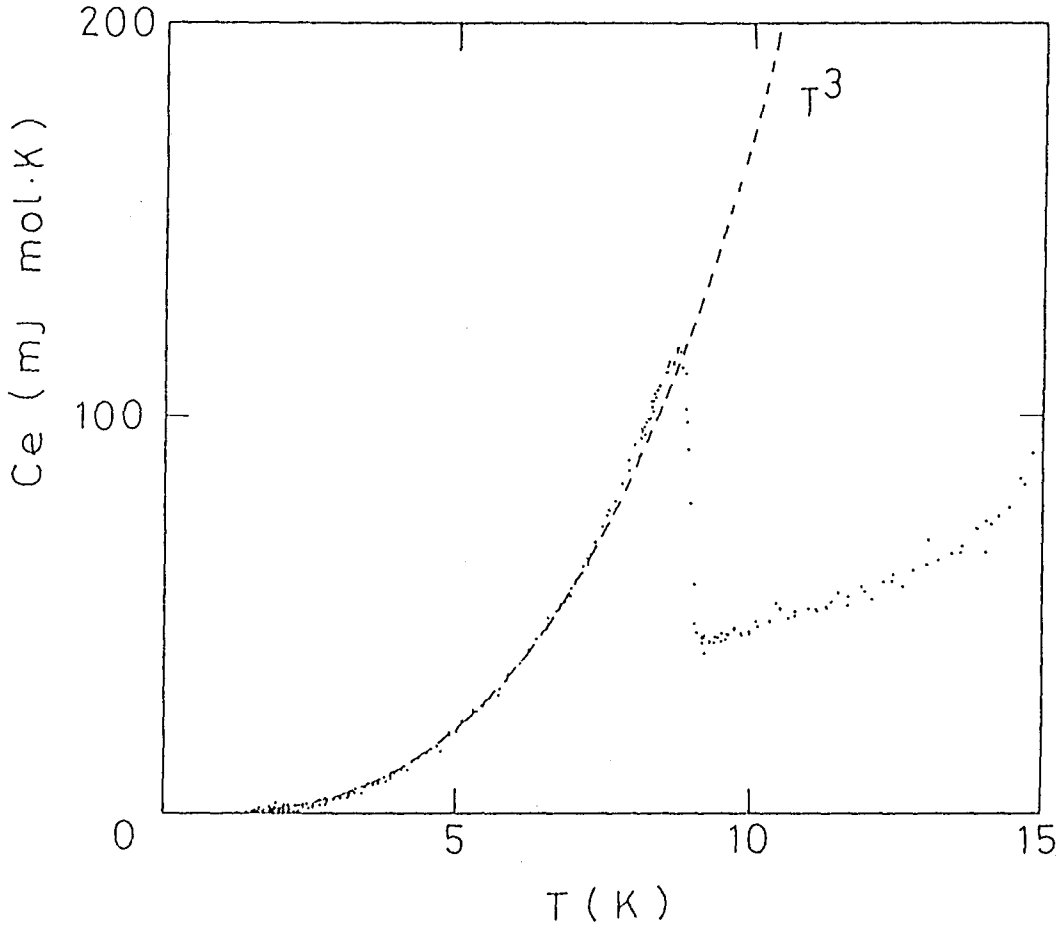

Fig. 1 (c) Eletronic specific heat data plotted versus T.

Table 1 Best fit parameters for specific heat in the normal state. The fitting temperature range is from 9.2K to 14.2K.

γ (mJ/mol K^2)	β (mJ/mol K^4)	α (mJ/mol K^6)	δ (mJ/mol K^8)
47.7	1.13	-2.76×10^{-3}	2.40×10^{-9}

where λ is the electron phonon coupling constant , n the number of the unit cells per mol and Θ_D the Debye temperature . The McMillan's formula[9] gives

$$T_C = (\Theta_D / 1.45) \exp (-1.04 (1 + \lambda) / \{ \lambda - \mu^* (1 + 0.62 \lambda) \}) , \quad (4)$$

where μ^* is the Coulomb pseudo potential. From the above values of γ and β , we obtain Θ_D = 120 K , λ = 1.36 and $N(E_F)$ = 3.69 state / eV · atom assuming μ^* = 0.13 .

The normalized electronic part of the specific heat can be estimated from Fig. 1(a) by subtracting the phonon part , and it is shown in Fig. 1(b). From this figure the specific heat jump $\Delta C / \gamma T_C$ is estimated to be 2.0. This value is not so far from 1.43 given by BCS theory and 1.20 calculated in the ABM state. As shown in Fig. 1(c), the electronic part of the specific heat is clearly proporional to T^3 at temperatures well below T_C, which is inconsistent with the BCS theory. This fact implies the superconducting energy gap is anisotropic and vanishes at points on the Fermi surface[10]. These investigations suggest that the "slightly heavy electron" takes part in the superconductivity .

§4. Nuclear Spin-Lattice Relaxation in the Normal State

A typical ^{51}V NMR lineshape is shown in Fig. 2 which consists of a narrow center peak and a wide wing broadened by the quadrupole interaction . The spin lattice relaxation time T_1 was estimated by fitting the measured recovery curve of the nuclear magnetization after the saturating comb pulses, $(M_0 - M(t))/M_0$ to the multi exponential function

$$(M_0 - M(t))/M_0 = 0.011\exp(-t/T_1) + 0.0682\exp(-6t/T_1) + 0.206\exp(-15t/T_1) + 0.710\exp(-28t/T_1) \quad (5)$$

under the initial condition that the center levels ($1/2 \leftrightarrow -1/2$) are only saturated [11]. Here, $M(t)$ and M_0 represent the nuclear magnetizatin at time t after the saturation pulses and at $t=\infty$, respectively. Examples of the magnetization recoveries with the best fit curves measured at 13 K and 77 K are plotted in Figs. 3 and 4, respectively.

The measured T_1 is shown in Fig. 5 by plotting $1 / T_1 T$ versus T in the temperature range from 9.2 K to 300 K. $1/T_1 T$, which reflects the density of states near the Fermi level, decreases drastically with increasing temperature though it is constant for normal metals. The peak near 110 K is considered to be due to the martensitic phase transition. HfV_2 undergoes a cubic to orthorhombic structural transition at about 120K, which is accompanied by a volume increase and anormalous behaviors of the resistivity, heat capacity and susceptibility[12]. This behavior is related to an electronically induced lattice instability.

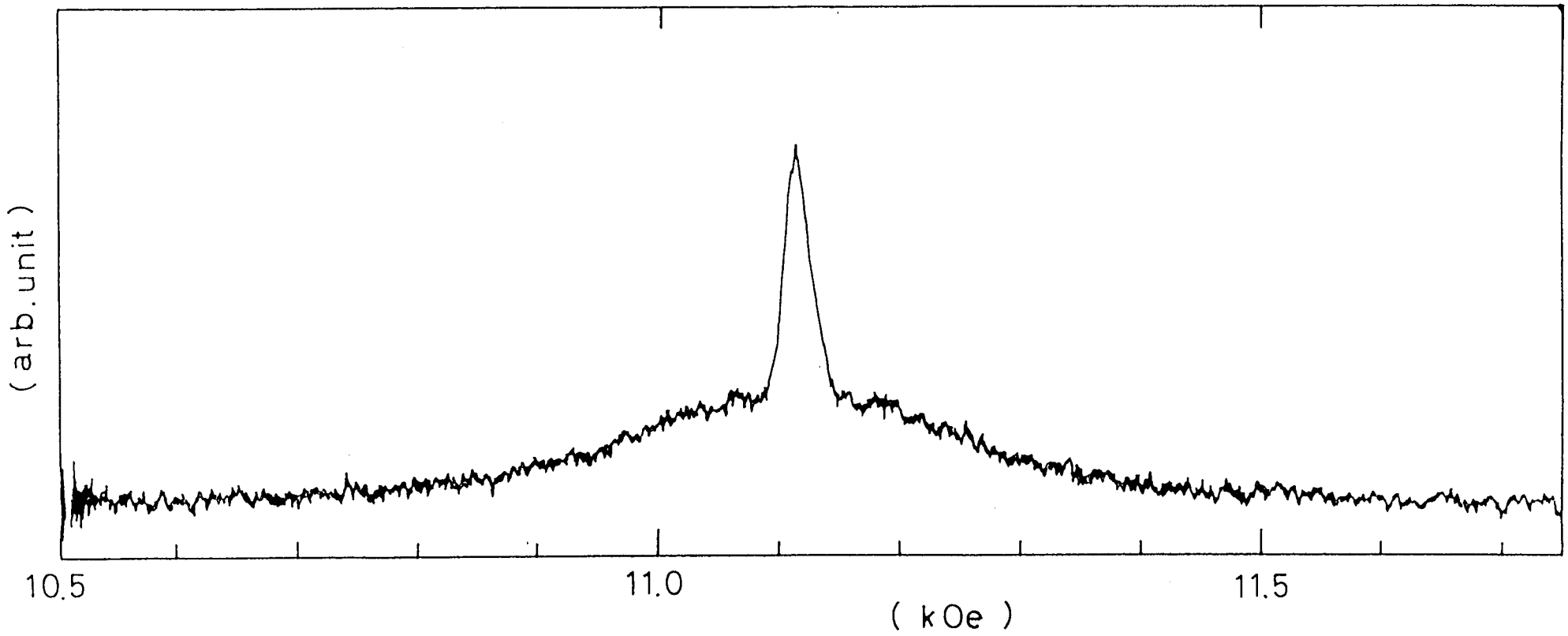

Fig. 2 ^{51}V spin echo spectrum of HfV_2 at 14.8 K.

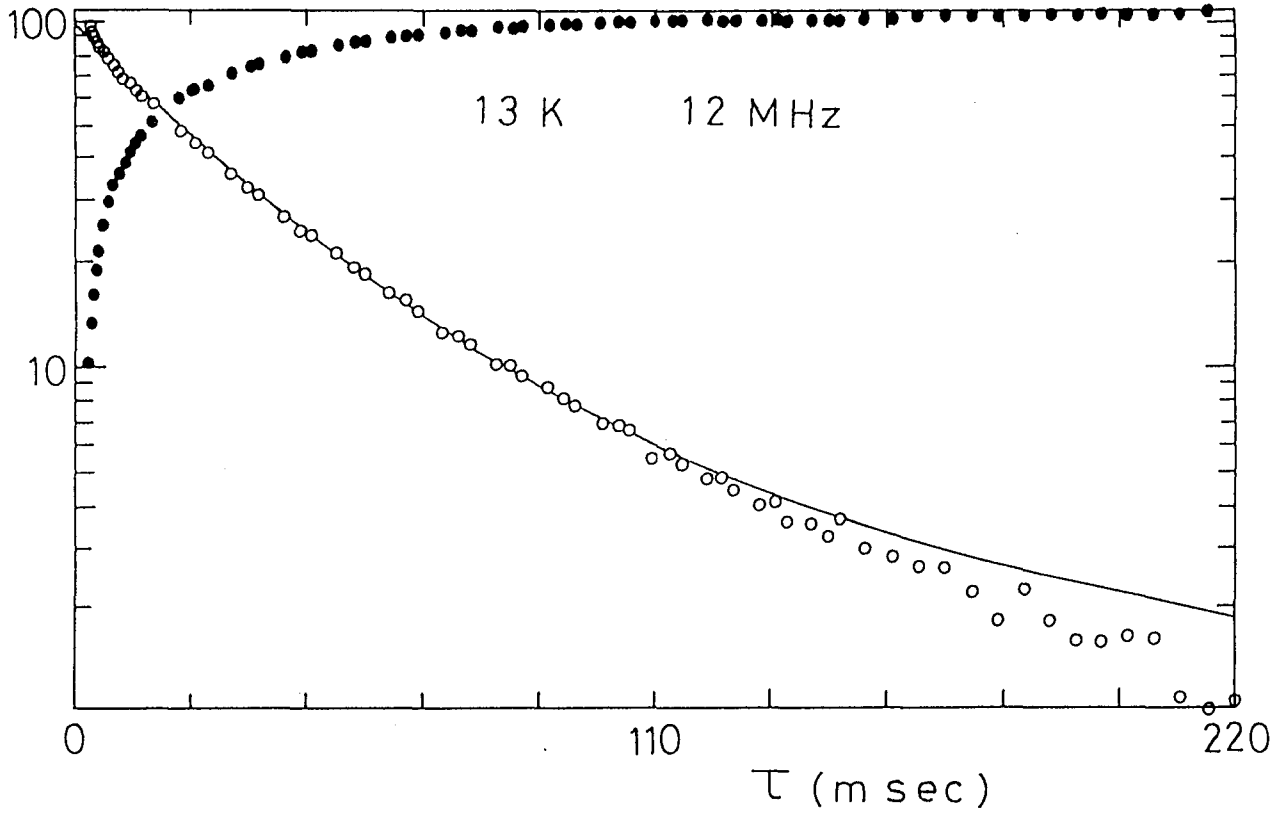

Fig. 3 Recoveries of the nuclear magnetization (closed circles) and the deviation from that in thermal equlibrium (open circles) at 13 K at 12 MHz. The solid curve is the best fit of eq. (5).

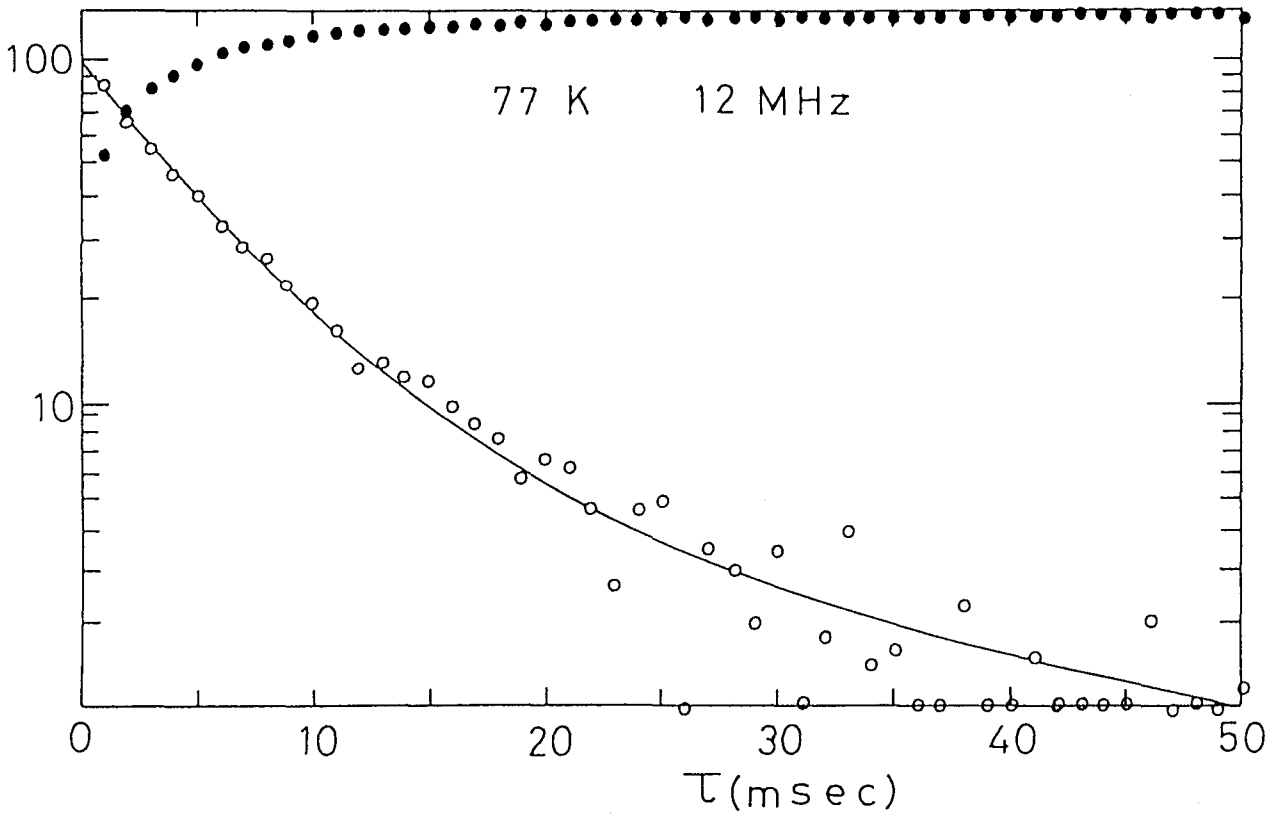

Fig. 4 Recoveries of the nuclear magnetization (closed circles) and the deviation from that in thermal equlibrium (open circles) at 77 K at 12 MHz. The solid curve is the best fit of eq. (5).

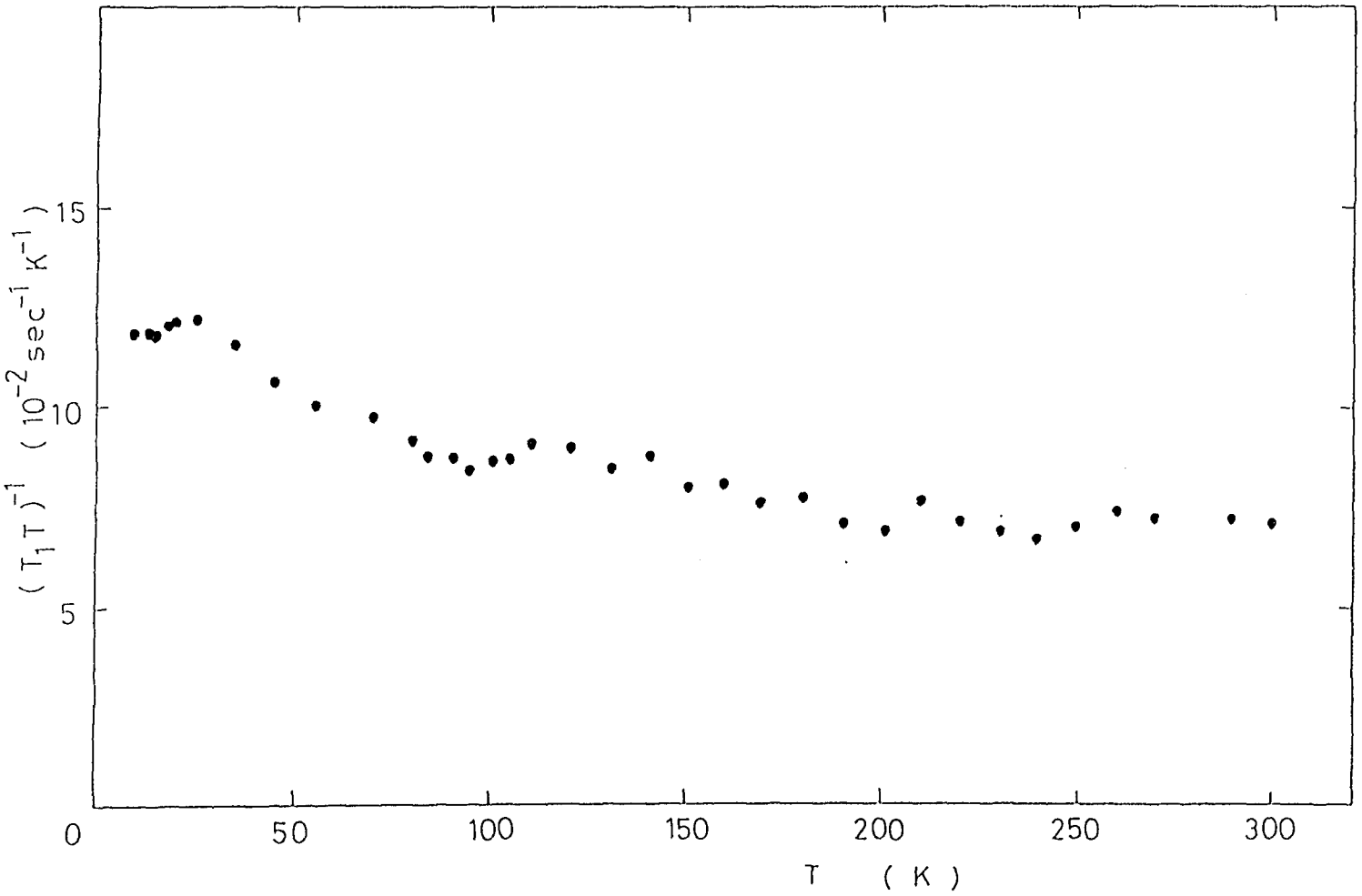

Fig. 5 Temperature dependence of $1/(T_1T)$ for ^{51}V in the normal state of HfV_2.

The observed $1/T_1$ represents the relaxation due to the d-spin fluctuation through the core polarization since the dipolar and the orbital relaxation mechanisms by d-electron can be neglected because of the crystal field in the C 15 structure. The large temperature dependence observed between 20 K and 100 K can be explained by the idea that the Fermi level acrosses a sharp narrow d-band with the half width of about 100 K. $1/T_1T$ appears to be constant between 9.4K and 20 K just above T_c, which may predict that the relation T_1T = const. is realized in the normal state below T_c .

In general, the relaxation rate $1/T_1$ due to the d-electron spin fluctuation is expressed in the form

$$1/T_1T \propto A^2 \int (N(E))^2 f(E)(1-f(E))dE, \qquad (6)$$

where A is the coupling constant, $N(E)$ the density of states of the d-electrons and $f(E)$ the Fermi distribution function. If $N(E)$ is known, $1/T_1T$ can be calculated. We tried to explain the observed behavior of $1/T_1T$ by the following two narrow band models :

1) $$N(E) = (3N/\sqrt{2}W^3)(W/\sqrt{2}+E_F+E)(W/\sqrt{2}-E_F-E), \qquad (7)$$

2) $$N(E) = (NW/2\pi)/((E_F+E)^2+(W/2)^2), \qquad (8)$$

where E_F is the Fermi energy, W the half width of their narrow bands, and N the total number of the electronic states. These models are illustrated in Fig. 6(a) and (b). In these figures the

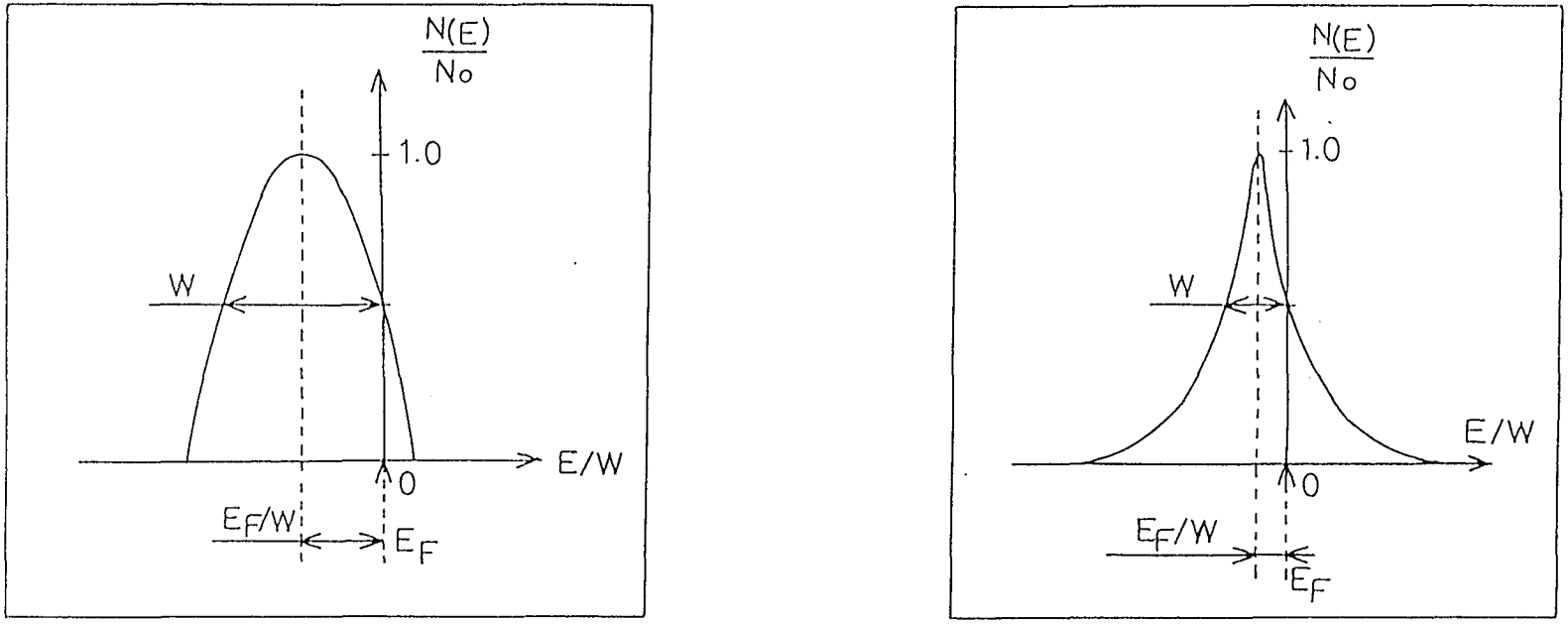

Fig. 6 Two models of the narrow density of states used in the calculation for $1/(T_1T)$.

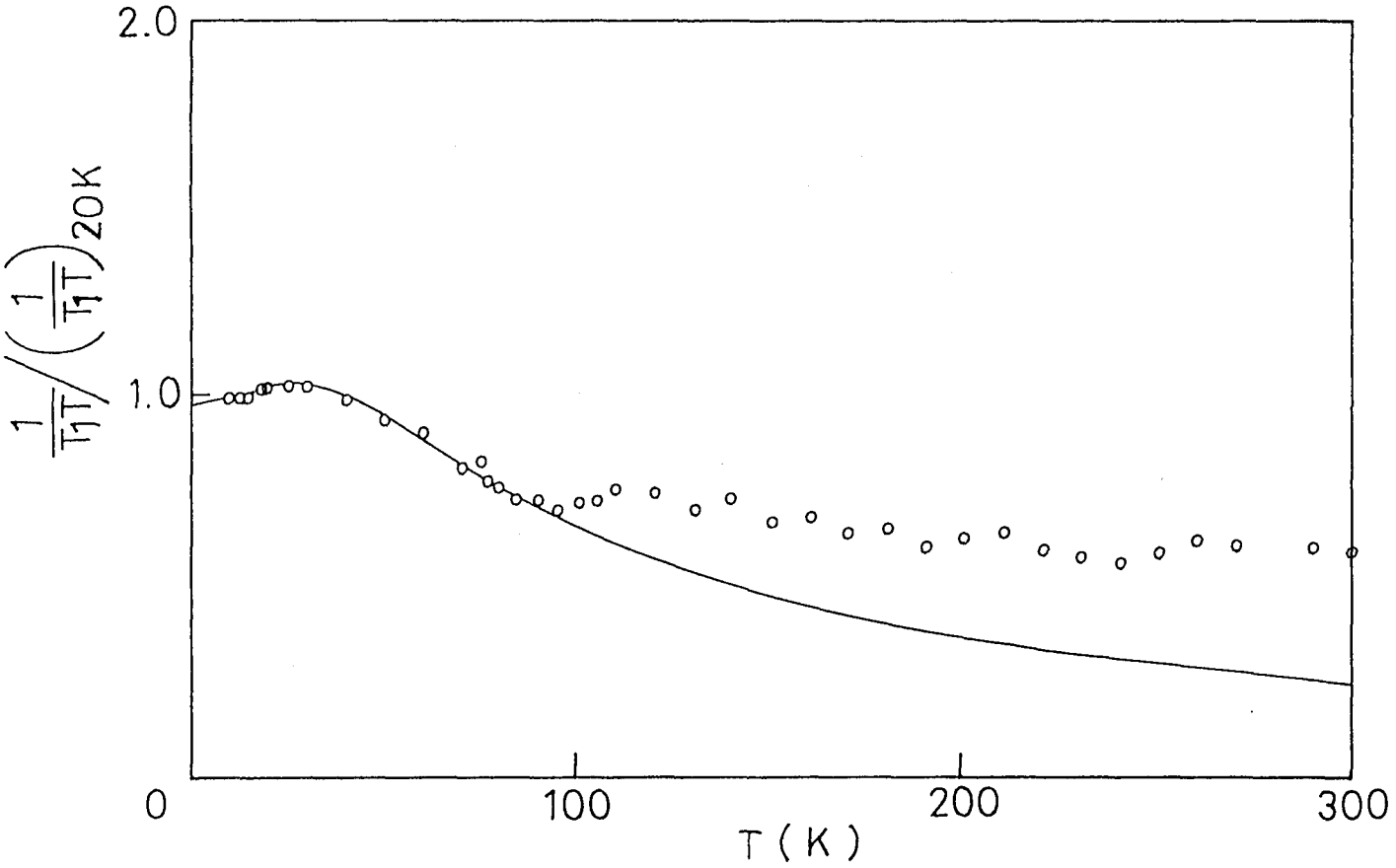

Fig. 7 Calculated $1/(T_1T)$ based on the density of states shown in Fig. 6. (a) (solid curve). Open circles represents the experimental data.

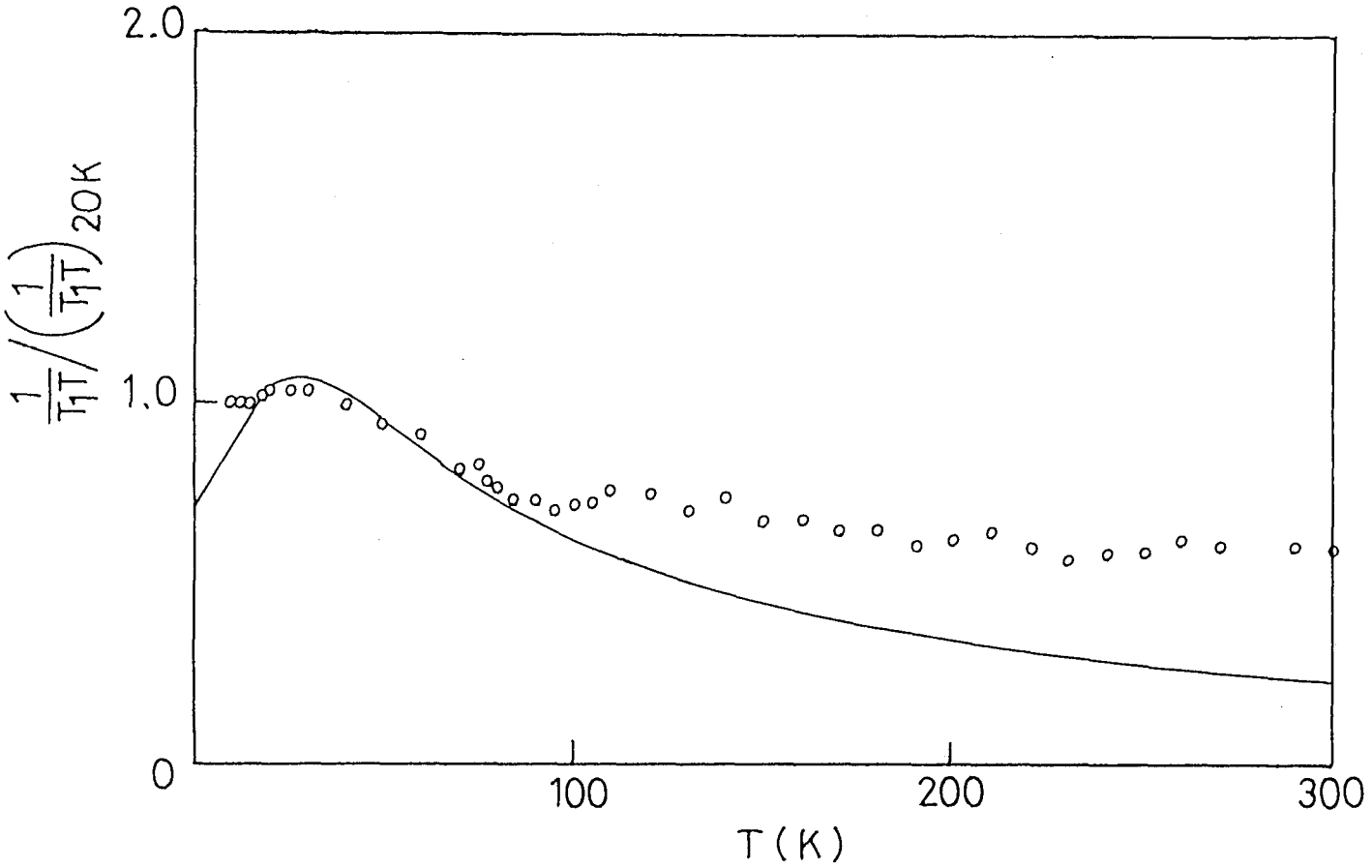

Fig. 8 Calculated $1/(T_1T)$ based on the density of states shown in Fig. 6.(b) (solid curve). Open circles represents the experimental data.

energy E=0 corresponds to the Fermi energy E_F, and these functions are normalized by the peak value N_0. The parameters E_F/W and W were determined so that the eqs. (7) and (8) fit to the data in Fig. 5. The best fit calculations are shown in Fig. 7 for the model (1) with the parameters W/k_B=141 and E_F/W=0.42, and in Fig. 8 for the model (2) with W/k_B=120 and E_F/W=0.5. In these figures, $1/T_1T$ is normalized by the value at 20 K. As shown in Figs. 7 and 8 , the agreement between the calculations and the experimental data is satisfactorily good in the temperature range from 20 K to 100 K. The deviation of the calculated curves from the experimental data at higher temperatures T>100 K may be caused by the change of the band structure accompanied by the martensitic phase transition. The model 1) fits to the data better than the model 2), which suggests the narrow band of the model 1) may represent the real band structure. Anyway, the temperature dependence of $1/T_1T$ at low temperatures (20 K< T < 100 K) can be explained by the narrow d-electron band of about 100 K due to the strong electron-phonon interaction.

§5. Nuclear Spin-Lattice Relaxation in the Superconducting State

5.1 T_1 Measured in the Constant External Field

In the temperature range of 1.4K to T_c, T_1 was measured in the same way as in the normal state. For the estimation of T_1 we used the same fitting function, eq. (5) as in the normal state. Examples of the magnetization recovery data with the best fit curves measured at 1.82 K and 4.2 K are shown in Figs. 9 and 10, respectively. The obtained data $1/T_1$ are plotted versus T in Fig. 11 together with the results in the normal state. $1/T_1$ shows a very small peak just below T_c and decreases rapidly with decreasing temperature. We also measured T_1 at different frequencies 6MHz and 3MHz in the temperature range from 1.4K to 4.2K. The obtained data are shown by closed circles and crosses, respectively, in Fig. 11. In Fig. 12, these data are plotted against T_c/T to show the frequency dependence of T_1 more clearly. From Fig. 11 and Fig. 12 we can say that the frequency dependence of $1/T_1$ is not large. This result conflicts with that by Silbernagel et al.[13]. The absence of the field dependence in the present measurement may be due to the fact that our sample has additional strains induced by cold working upon filing and that they eliminate the spin diffusion mechanism[14]. In Fig. 11, all these data measured at 12 MHz, 6MHz and 3MHz are nearly on the straight line which shows the T^5 dependence. That is, $1/T_1$ is nearly proportional to T^5 in the temperature range well below T_c and inconsistent with the exponential $(-1/T)$ dependence predicted by the BCS theory[6,15]. In Fig. 13(a) and (b) we tried to plot the

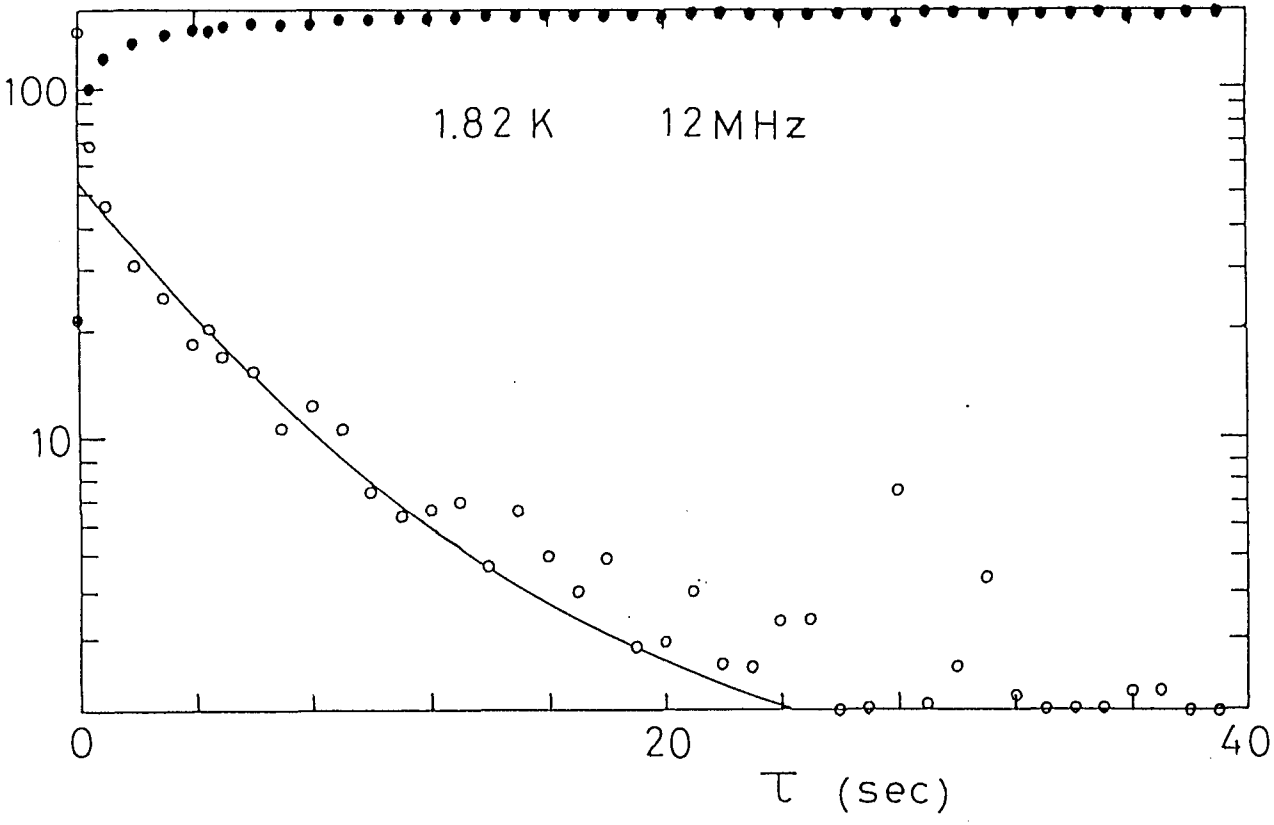

Fig. 9 Recoveries of the nuclear magnetization (closed circles) and the deviation from that in thermal equlibrium (open circles) at 1.82 K at 12 MHz. The solid curve is the best fit of eq. (5).

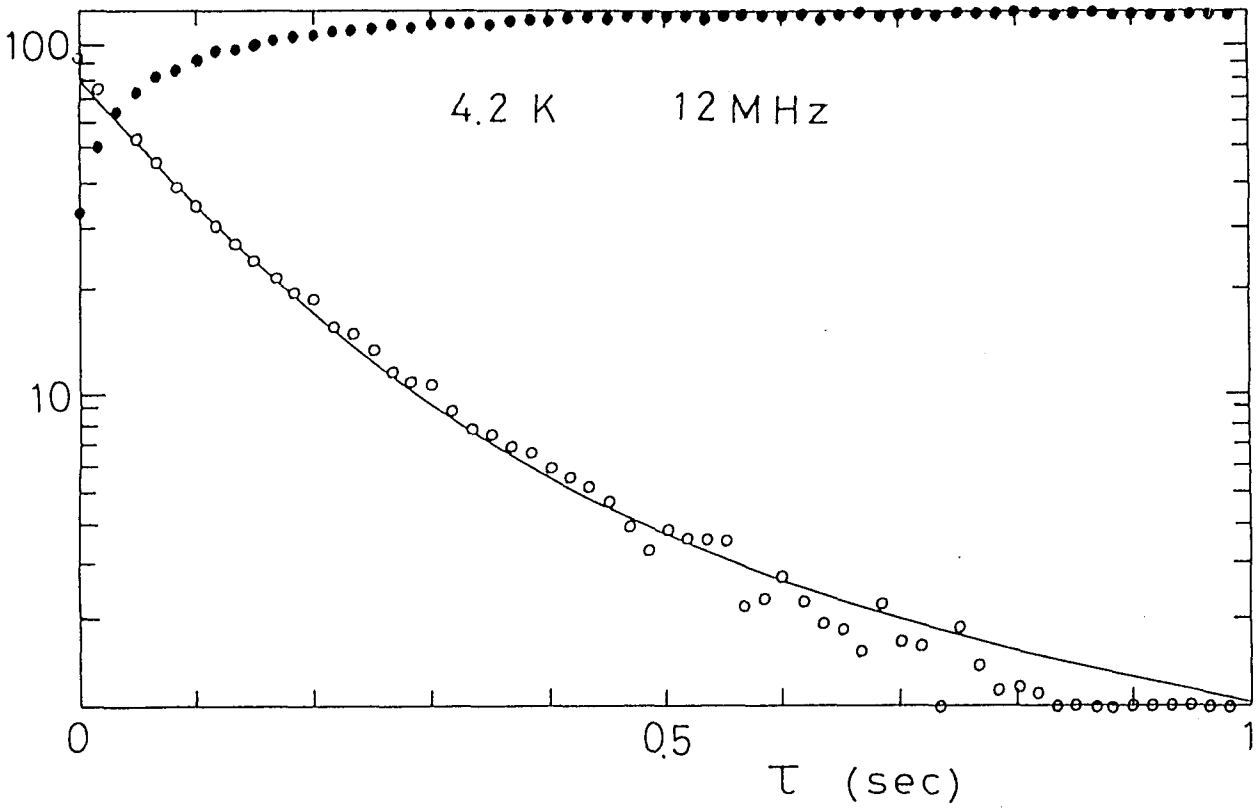

Fig. 10 Recoveries of the nuclear magnetization (closed circles) and the deviation from that in thermal equlibrium (open circles) at 4.2 K at 12 MHz. The solid curve is the best fit of eq. (5).

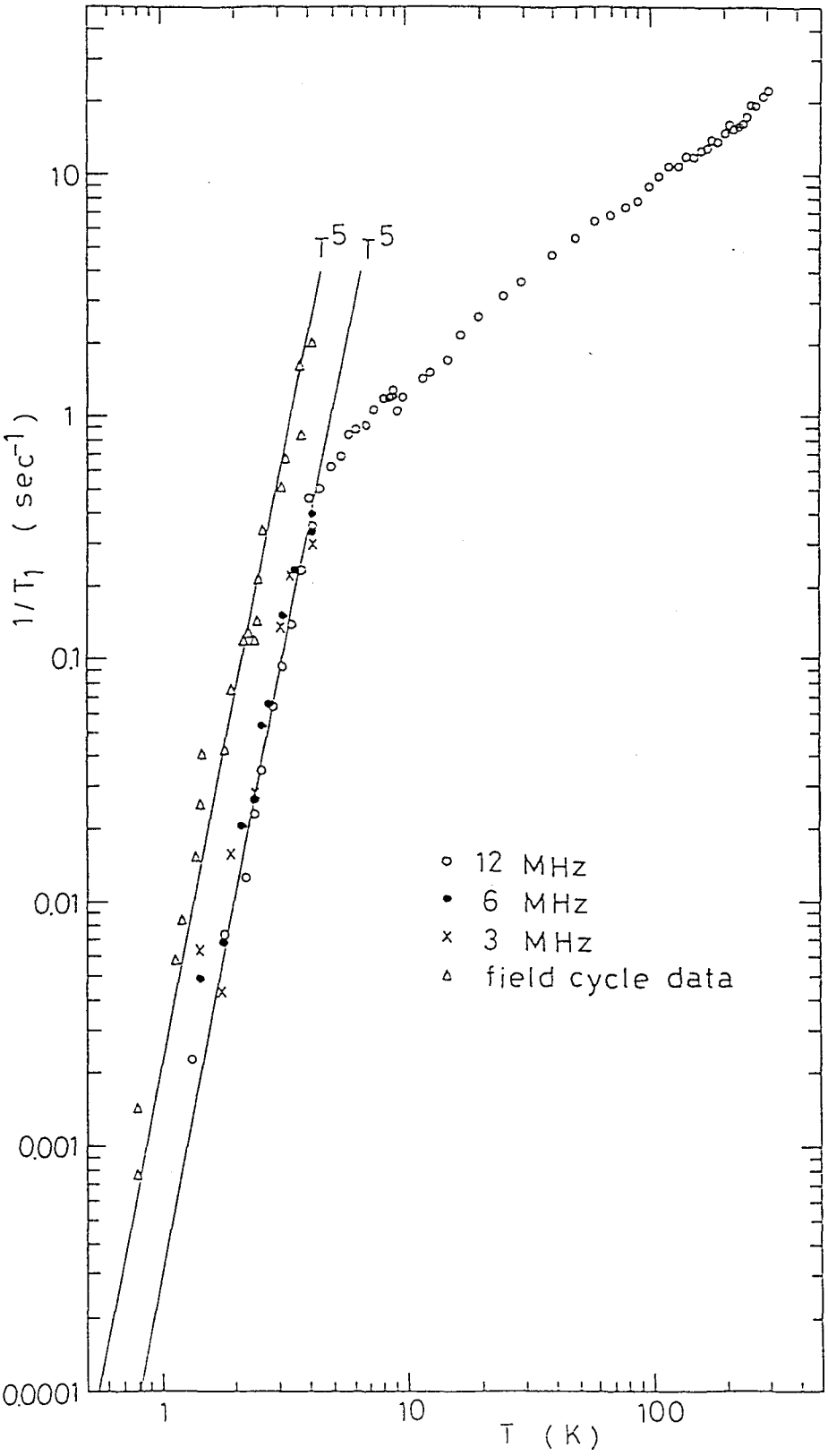

Fig. 11 Temperature dependence of $1/T_1$ measured at 12 MHz (open circles), 6 MHz (closed circles) and 3 MHz (crosses). Data measured by the field cycle method are also shown by triangles. The solid curves show the T^5 dependence.

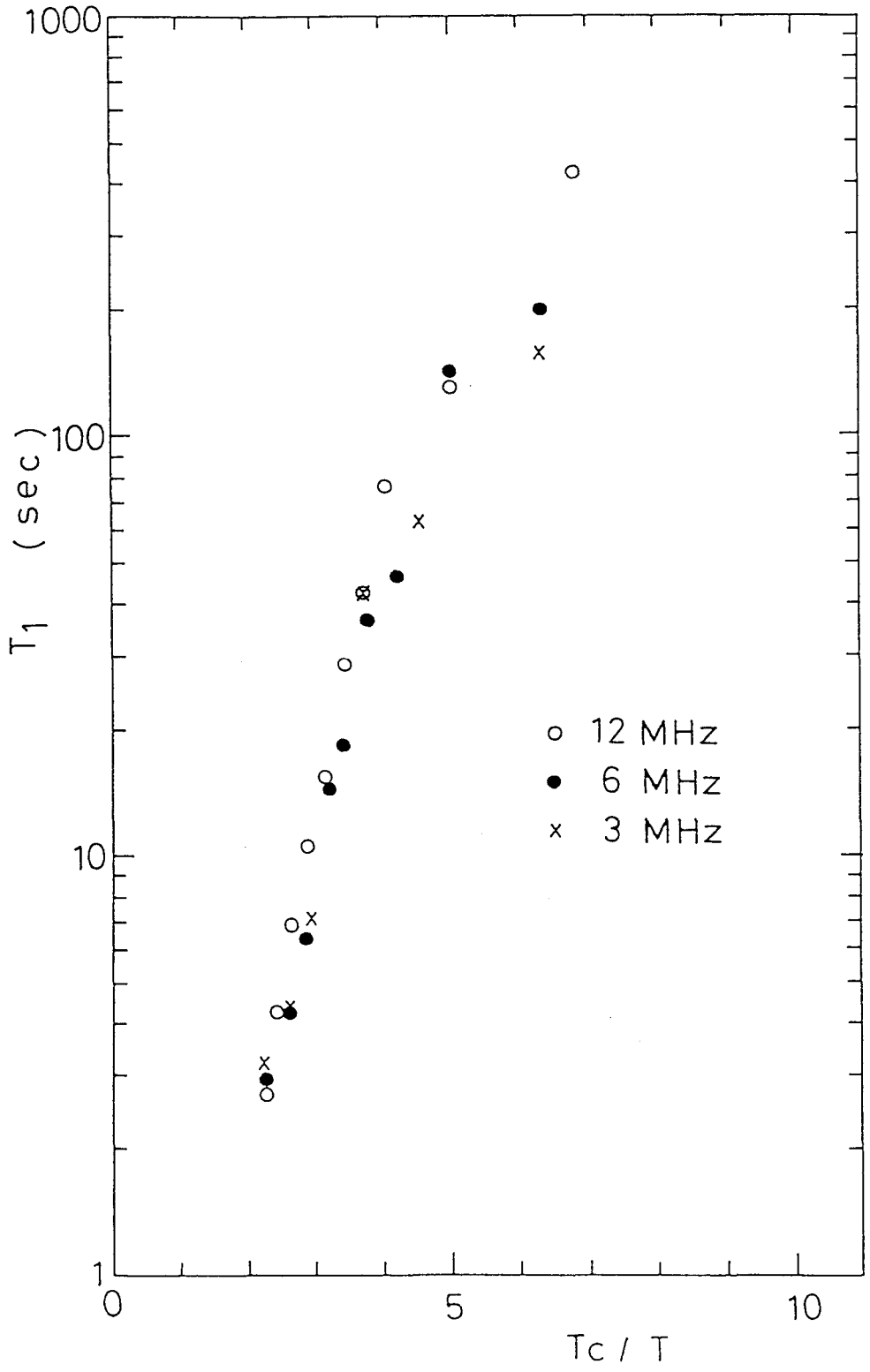

Fig. 12 A plot of T_1 as a function of T_c/T at 12 MHz (open circles), 6 MHz (closed circles) and 3 MHz (crosses).

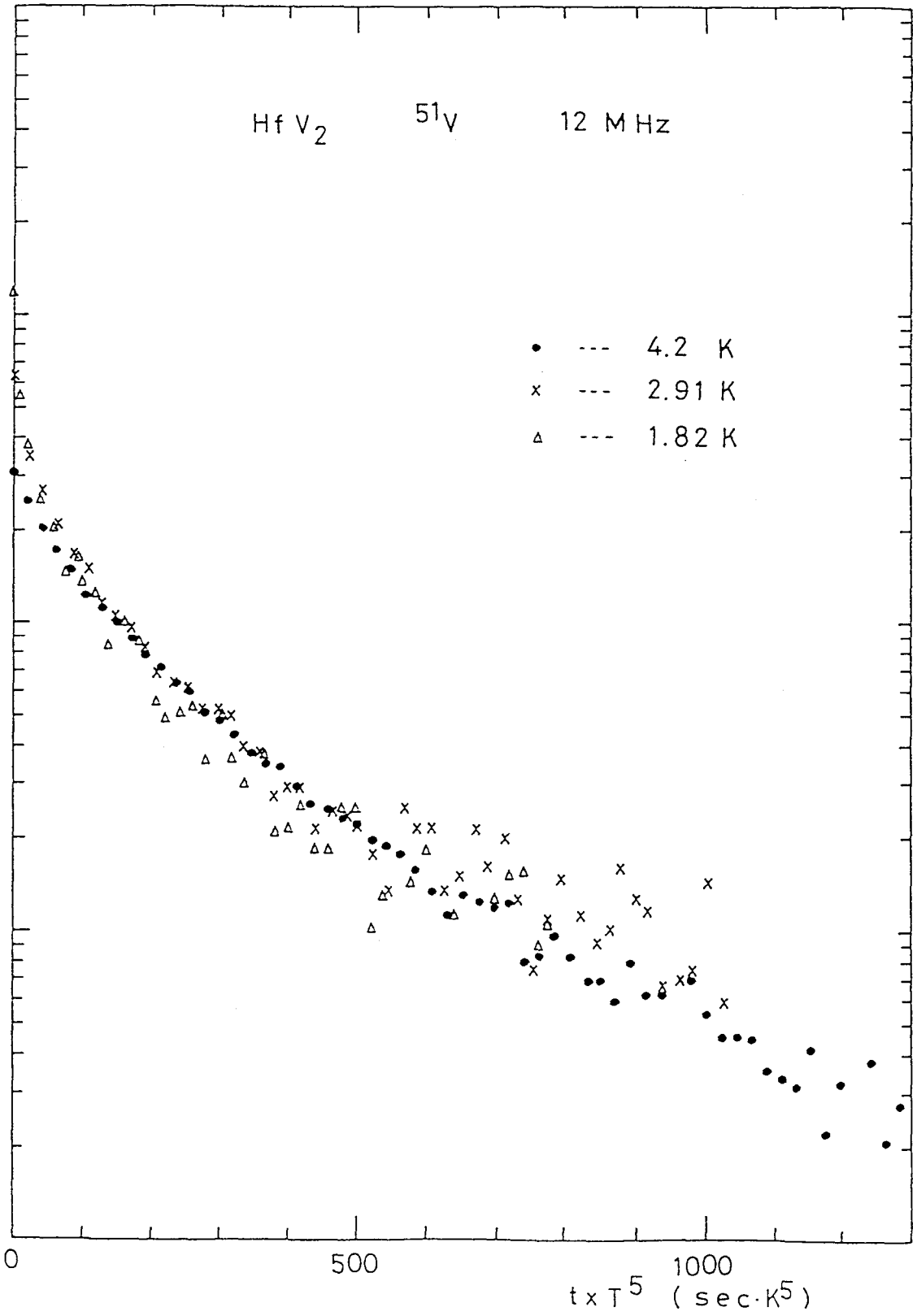

Fig. 13 (a) Magnetization recoveries measured at different temperaturs are plotted against tT^5.

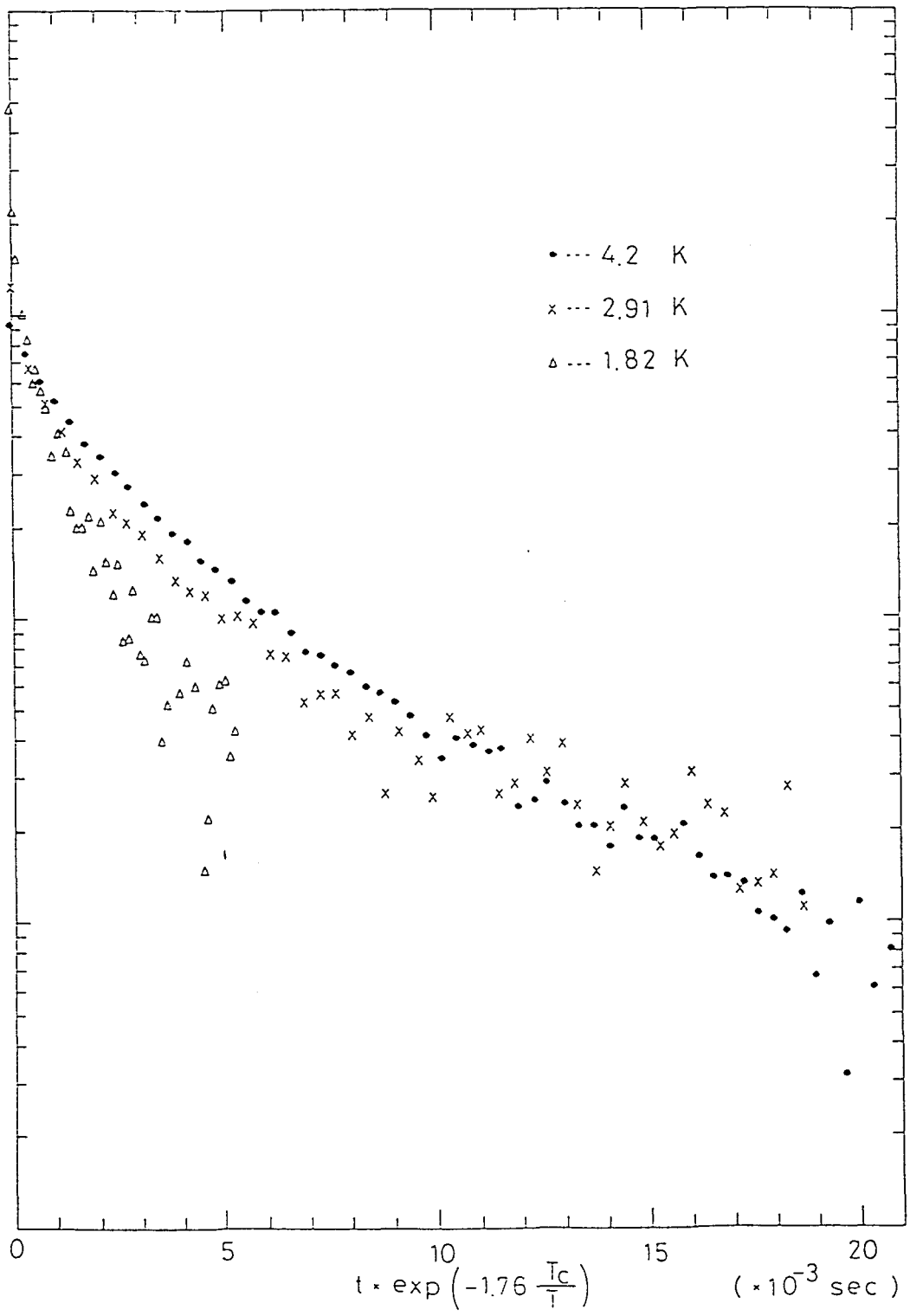

Fig. 13 (b) Magnetization recoveries measured at different temperaturs are plotted against $t \cdot \exp(-1.76 T_c/T)$

magnetization recoveries measured at some different temperatures, 4.2K, 2.9K and 1.82 K at the resonance frequency 12MHz on the same figure, in which the horizontal axis is scaled to tT^5 and $t\cdot\exp(-1.76T_C/T)$, respectively. The experimental points show the nearly same recovery in Fig. 13(a), while different ones in Fig. 13(b), which confirms $1/T_1 \propto T^5$.

We show the theoretical curves based on the ABM theory in Fig. 14(a). The broken curve is the prediction with energy gap parameter $\Delta(0)/k_B T_C=2.014$ and the solid curve is the best fit to the data with $\Delta(0)/k_B T_C=2.014\times0.8$. In Fig. 14(b), the theoretical curves based on the BCS theory are shown. The broken curve is the prediction with energy gap parameter $\Delta(0)/k_B T_C=1.76$ and the energy broadening $\delta E=0.1\Delta(T)$, and the solid curve is the best fit to the data with $\delta E=0.67\Delta(T)$. The $1/T_1$ does not depend on the detailed feature of the anisotropic energy gap but on the root mean square of the anisotropic energy gap[18]. The anisotropic energy gap $\Delta(\Omega)$ is expressed as

$$\Delta(\Omega) =\langle\Delta\rangle\cdot\{1+a(\Omega)\}, \qquad (9)$$

where $\langle\Delta\rangle$ is the average of the energy gap and $a(\Omega)$ denotes the angular variation of the gap over the Fermi surface. In the ABM state the root mean square anisotropy $(\langle a^2\rangle)^{1/2}$ is calculated to be 0.284. This value corresponds to the energy broadening of $\delta E=0.50\Delta(T)$ in the BCS theory. $1/T_1$ is sensitive to the low energy part of the square of the density of states, $(N_S(E))^2$ at low temperature. As the energy broadening in the BCS state becomes

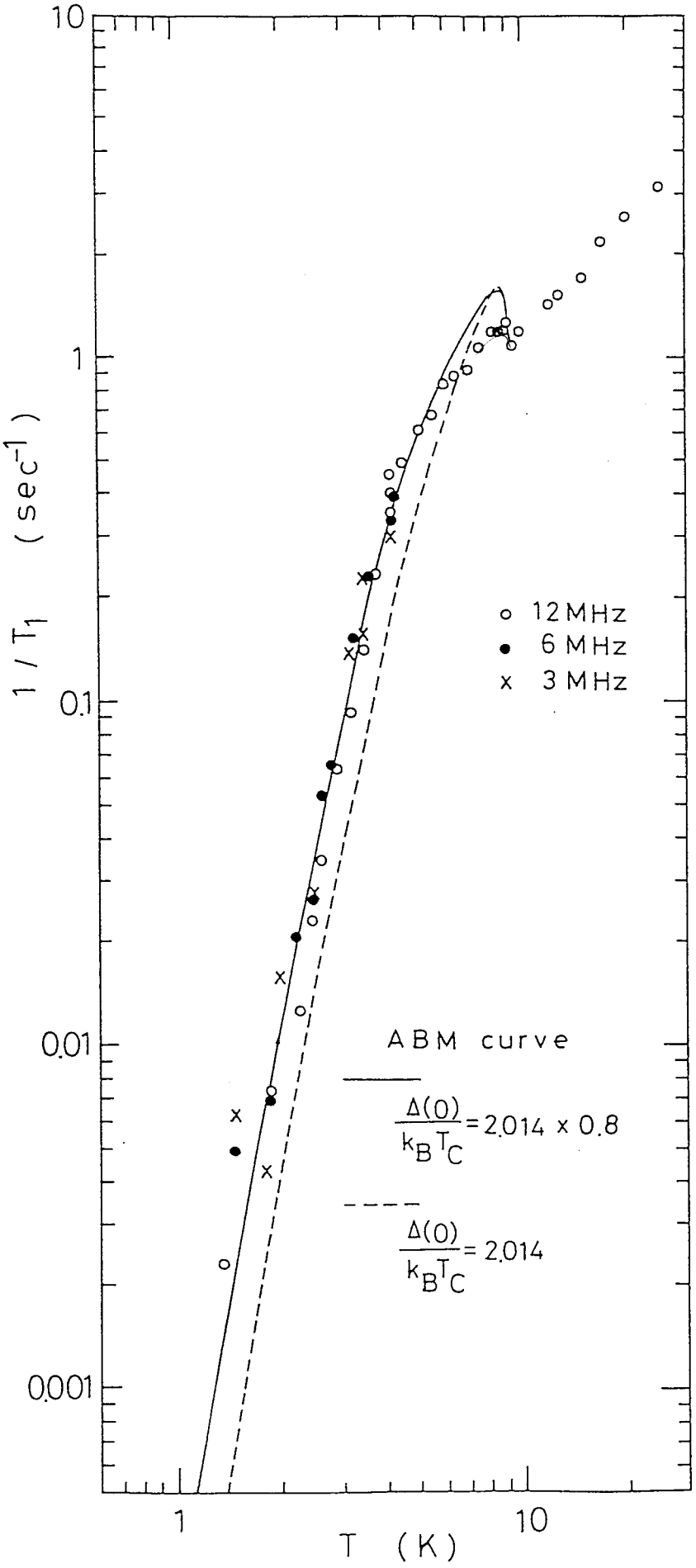

Fig. 14 (a) Calculated curves of $1/T_1$ based on the ABM model with the gap parameter $\Delta(0)/k_B T_C = 2.014$ (dashed curve) and $\Delta(0)/k_B T_C = 2.014 \times 0.8$ (solid curve).

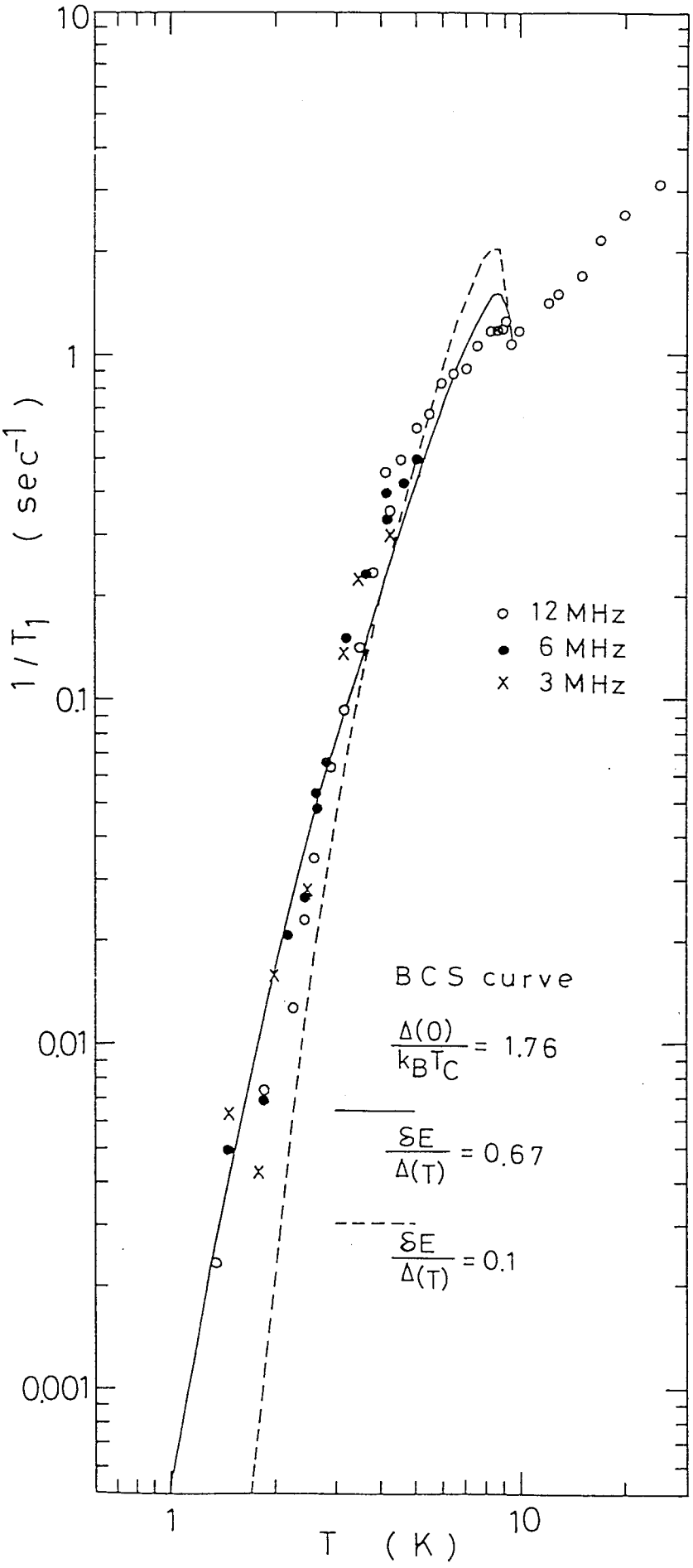

Fig. 14 (b) Calculated curves of $1/T_1$ based on the BCS model with the gap parameter $\Delta(0)/k_B T_C = 1.76$ and energy broadening $\delta E/\Delta(T) = 0.5$ (dashed curve), and $\delta E/\Delta(T) = 0.67$ (solid curve).

larger, the density of states for the BCS state at low temperature approaches to that for the ABM state[19]. In order to explain the temperature dependence of the obtained data by the BCS theory, I need to introduce as much as 67 % energy broadening. It is more reasonable to introduce an ABM anisotrpy than such a large energy broadening. Actually, the agreement between the data and the ABM curve with $\Delta(0)/k_B T_C = 2.014 \times 0.8$ is satisfactorily good at low temperature. The reason of this reduction of the gap parameter is not clear at present. The leading term of $1/T_1$ has T^5 dependence at low temperature, which has been shown in Fig. 11.

The fact that the BCS curve approaches to the data with increasing the energy broadening δE can be understood as follows. Figures 15(a) and (b) show the BCS energy gap model with δE and the ABM energy gap model at the Fermi surface, respectively. From this figure, I can say that the gap papameter Δ_0 in the BCS model corresponds to $\langle\Delta(\Omega)\rangle$ in the ABM model. At low temperature Δ_0 is replaced by $\Delta(0)$, and in the ABM model $\langle\Delta(\Omega)\rangle$ is given by $\pi/4 \cdot \Delta_{0\ ABM} = 0.785 \times 2.014 k_B T_C = 1.58 k_B T_C$. Thus $\langle\Delta(\Omega)\rangle$ corresponds to about 90 % of Δ_0 for the BCS state ($\Delta_0 = 1.76 k_B T_C$). In Fig. 16, $(N_S(E/\Delta))^2$ in the BCS model with $\delta E = 0.5\Delta(T)$ is shown by crosses, and with $\delta E = 0.67\Delta(T)$ by triangles, and that in the ABM model by closed circles. As shown in this figure, the behavior of $(N_S(E/\Delta))^2$ of the BCS model with $\delta E = 0.5\Delta(T)$ resembles that of the ABM model. Because $\langle\Delta(\Omega)\rangle = 0.9\Delta_0$, one should extend the horizontal axis of Fig. 16 for the BCS state by the factor 1/0.9. Therefore, I can say that $(N_S(E/\Delta))^2$ for the BCS model with $\delta E = 0.67\Delta(T)$ is very near to that for the ABM model.

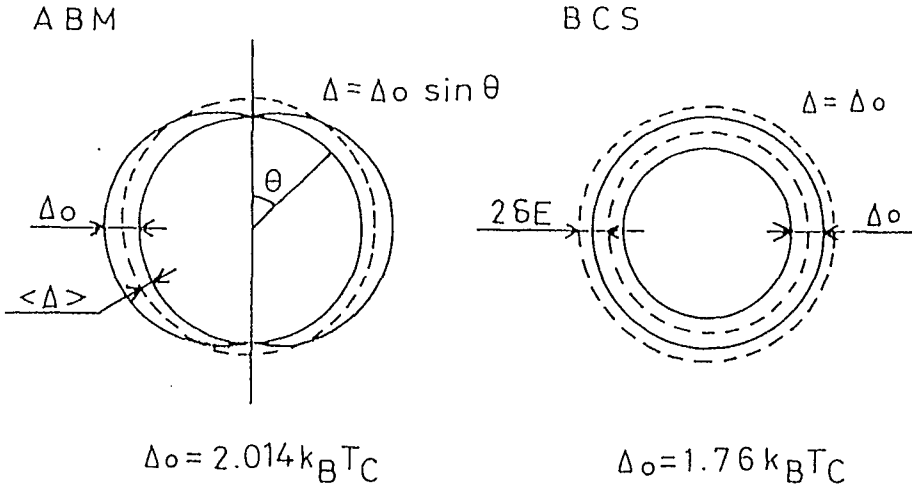

Fig. 15 (a) Energy gap of the ABM model at Fermi surface
(b) Energy gap of the BCS model at Fermi surface

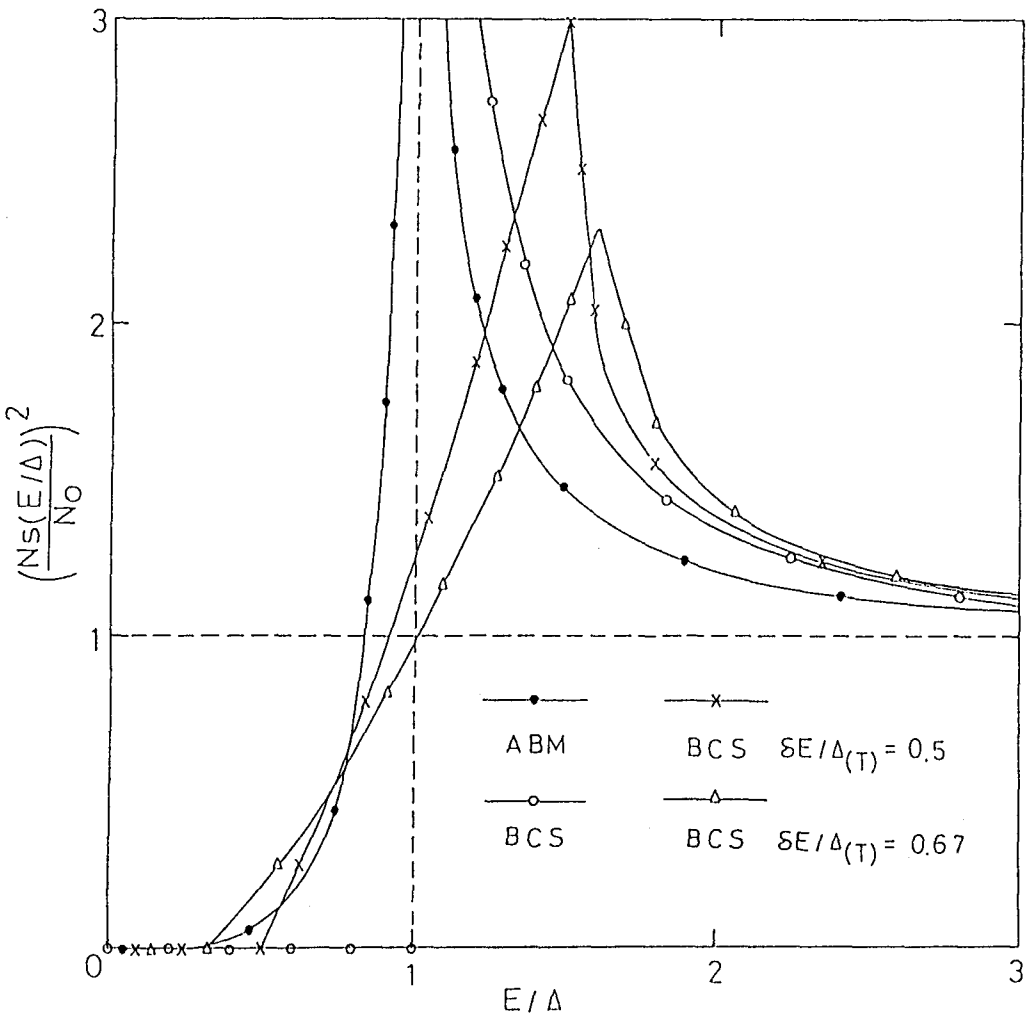

Fig. 16 Comparison of $(N_s(E/\Delta)/N_0)^2$ in the ABM model (closed circles), BCS models with $\delta E/\Delta(T)=0$ (open circles), $\delta E/\Delta(T)=0.5$ (crosses) and $\delta E/\Delta(T)=0.67$ (triangles)

5.2 Field Cycle Method

When we measure T_1 in the applied external magnetic field, the distribution of the spin-lattice relaxation time due to the vortex and the spin diffusion mechanism make the magnetization recovery curve complex, so that it is desirable to measure T_1 in the zero field condition. In Fig. 17, the time table of the field cycle method is shown. The applied field is initially kept H_0 in the resonance condition for at least ten times of the relaxation time. Then, the field is reduced to zero. After a time interval τ, the field is turned on back to H_0 again. These demagnetization and remagnetization processes must be adiabatic. In this zero field, the nuclear spins relax during this time interval τ . The initial nuclear magnetization at $\tau=0$ is the same as that in the field H_0. The nuclear magnetization decreases with increasing τ and becomes zero after sufficiently longer time τ than T_1. We can measure T_1 at zero field from the τ dependence of the magnetization.

Because we observe the central resonance line ($1/2 \leftrightarrow -1/2$) of ^{51}V nuclei after the remagnetization, we can use the rate equation proposed by Narath[11]. This rate equation is given by

$$da_m(t)/dt = W \Sigma A_{m\,m'}\, a_{m'}(t) \quad , \qquad (10)$$

where $a_m(t)$ represents the deviation of the population difference of the adjacent $(m \leftrightarrow m-1)$ levels from that in the equilibrium state, and W is the transition probability between the adjacent $(m \leftrightarrow m-1)$ levels divided by $(I(I+1)-m(m-1))$. Using the matrix

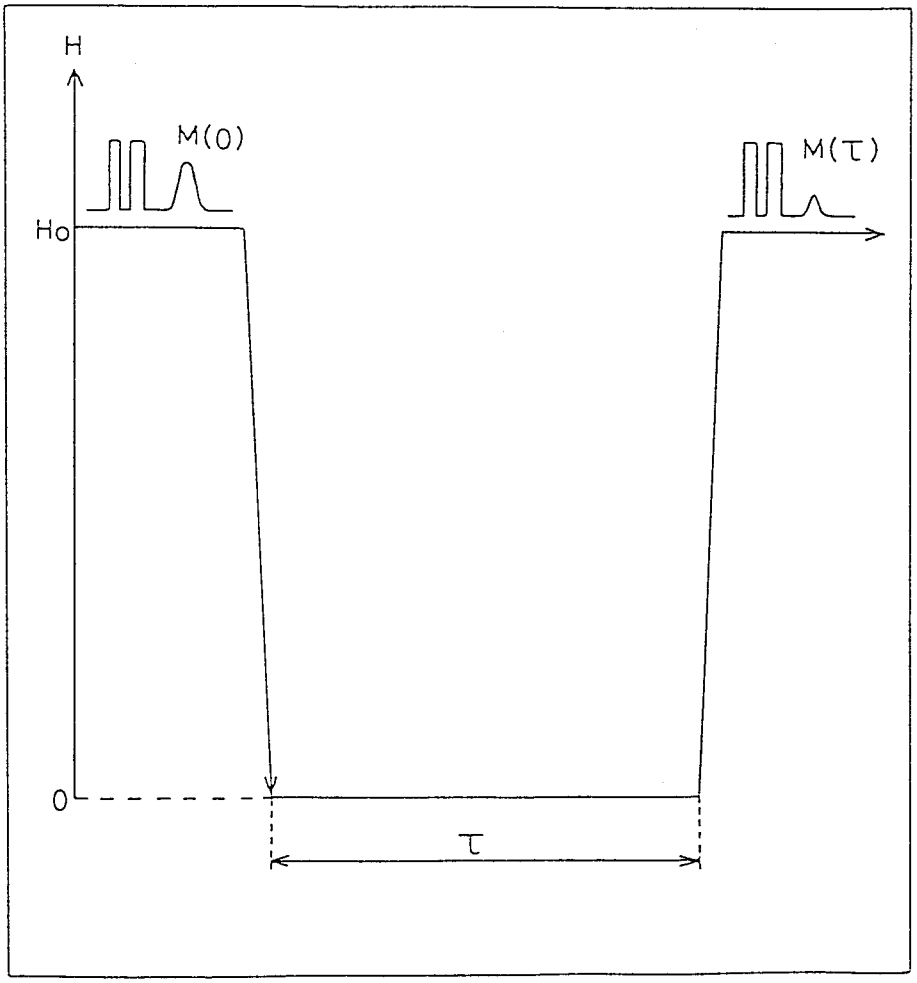

Fig. 17 Time table of the applied field in field cycle method

elements $A_{mm'}$ calculated for ^{51}V nucleus (I=7/2) by Narath[11], we obtain

$$a_{1/2}(t)=A\exp(-t/T_1)+B\exp(-6t/T_1)+C\exp(-15t/T_1)+D\exp(-28t/T_1), \quad (11)$$

where the coefficients A, B, C and D depend on the initial condition of the magnetization decay and are given as,

$$A=0.08333a_{-5/2}(0)+0.14285a_{-3/2}(0)+0.17857a_{-1/2}(0)+0.19047a_{1/2}(0)+0.17857a_{3/2}(0)+0.14285a_{5/2}(0)+0.08333a_{7/2}(0),$$

$$B=-0.5\times(0.31818a_{-5/2}(0)+0.09091a_{-3/2}(0)-0.22727a_{-1/2}(0)-0.36363a_{1/2}(0)-0.22727a_{3/2}(0)+0.09091a_{5/2}(0)+0.31818a_{7/2}(0)),$$

$$C=0.09615a_{-5/2}(0)-0.21978a_{-3/2}(0)+0.01373a_{-1/2}(0)+0.21978a_{1/2}(0)+0.01373a_{3/2}(0)-0.21978a_{5/2}(0)+0.09615a_{7/2}(0),$$

$$D=-8.75\times(0.00233a_{-5/2}(0)-0.01398a_{-3/2}(0)+0.03496a_{-1/2}(0)-0.04661a_{1/2}(0)+0.03496a_{3/2}(0)-0.01398a_{5/2}(0)+0.00233a_{7/2}(0), \quad (12)$$

where $a_m(0)$ is the initial population difference between the adjacnt levels m and m-1. If the initial populations of the

nuclear spin levels are the same as those in the Zeeman split state with a small population difference due to the quadrupolar energy, we can give $a_m(0)$ as

$$a_m(0)=\xi_0+\xi_Q(m-1/2), \tag{13}$$

where $\xi_0=\gamma_n\hbar H_0/k_B T$ represents the population difference due to the Zeeman energy $\gamma_n\hbar H_0$, and $\xi_Q=1/k_B T\cdot 3e^2qQ(3\cos^2\theta+1)/4I(2I-1)$ that originates from the quadrupolar interaction. Under this initial condition, we obtain

$$a_{1/2}(t)=a_{1/2}(0)\exp(-t/T_1). \tag{14}$$

The field cycle method was employed in order to measure T_1 in the zero field condition in the temperature range of 0.77K to 4.2K. Figure 18 shows an example of the magnetization decay data at 1.47K. This decay is not single exponential and the nuclear magnetization at $\tau=\infty$ is not zero. This suggests that the experimental demagnetization and remagnetization processes are not completely adiabatic and the populations of the nuclear spin levels are changing during these processes. The initial condition of the magnetization decay can not be known, so that we estimated T_1 by fitting the following equation,

$$(M_0-M(t))/M_0=A\cdot\exp(-t/T_1)+B\cdot\exp(-6t/T_1)+C\cdot\exp(-15t/T_1)+D\cdot\exp(-28t/T_1), \tag{15}$$

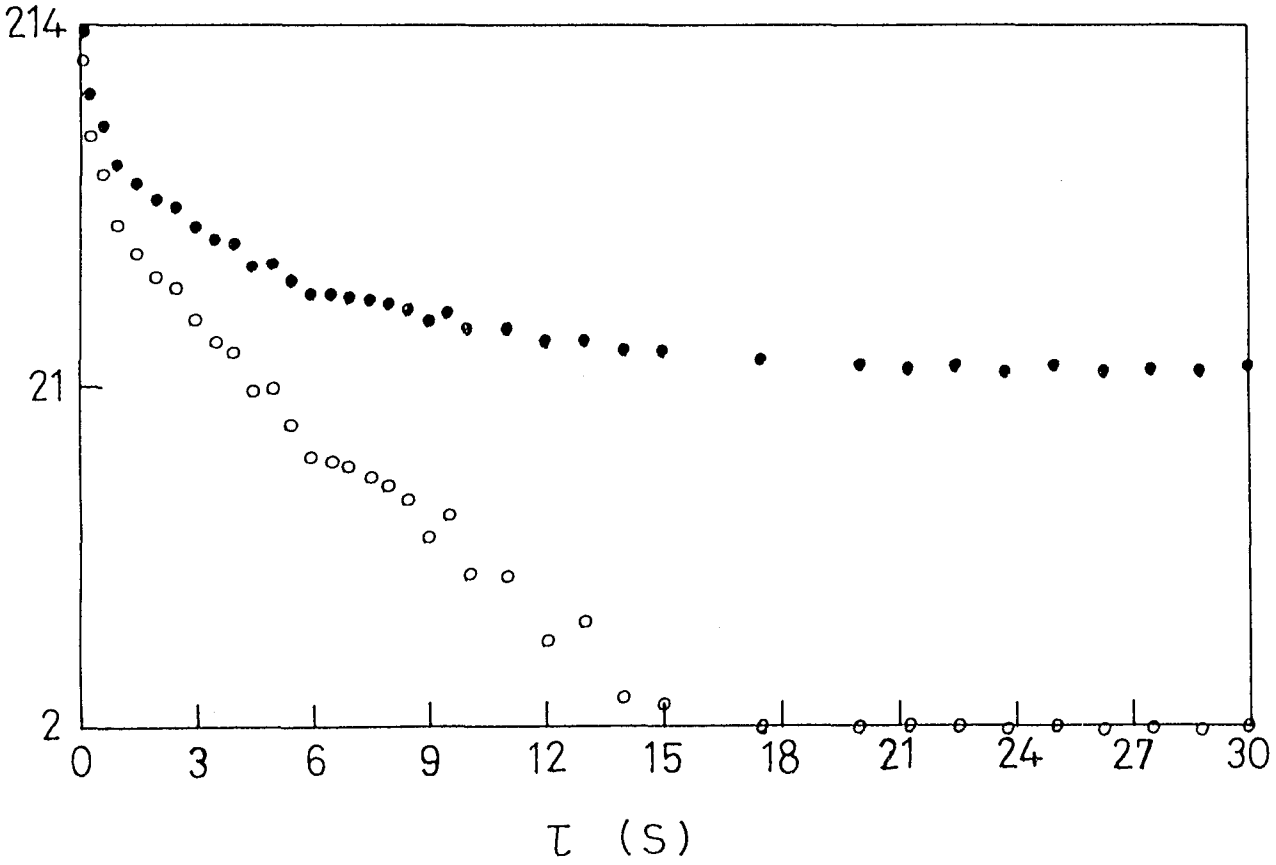

Fig. 18 An example of the nuclear magnetization decay (closed circles) and the substantial magnetization decay obtained by subtracting the value at sufficiently long τ (open circles) in the field cycle method.

where the coefficients of the exponential terms were also treated as unkown parameters. Two examples of the magnetization recoveries with the best fit curves measured at 1.14 K and 3.14 K in Figs. 19 and 20, respectively.

The best fit ratios of the parameters *A*, *B*, and *C* to *D* are tabulated in Table 2. These ratios vary with temperature, which shows that the initaial conditions are different at different temperatures. The values of *A* are negligibly small at any temperature. The *B* has a tendency to increase with increasing temperature. At 4.2 K the ratio A:B:C:D is close to that of 0.0167:0.955:0.289:1 in which only the NMR central line ($1/2 \leftrightarrow -1/2$) is saturated. It appears that the deviation of the populations of all the levels from the initial equilibrium state becomes larger with decreasing temperature. The obtained data $1/T_1$ are plotted in Fig. 11 by triangles together with the results measured in the constant magnetic field. These values of $1/T_1$ measured by the field cycle method are about 6.4 times as large as those measured in the constant magnetic field, about which some discussions will be given later. These triangles are also nearly on the straight line of T^5 dependence and far from the $\exp(-1/T)$ dependence predicted by the BCS theory. These facts suggest the superconducting energy gap is anisotropic and vanishes at points on the Fermi surface in HfV_2, which is consistent with the result of the specific heat measurement.

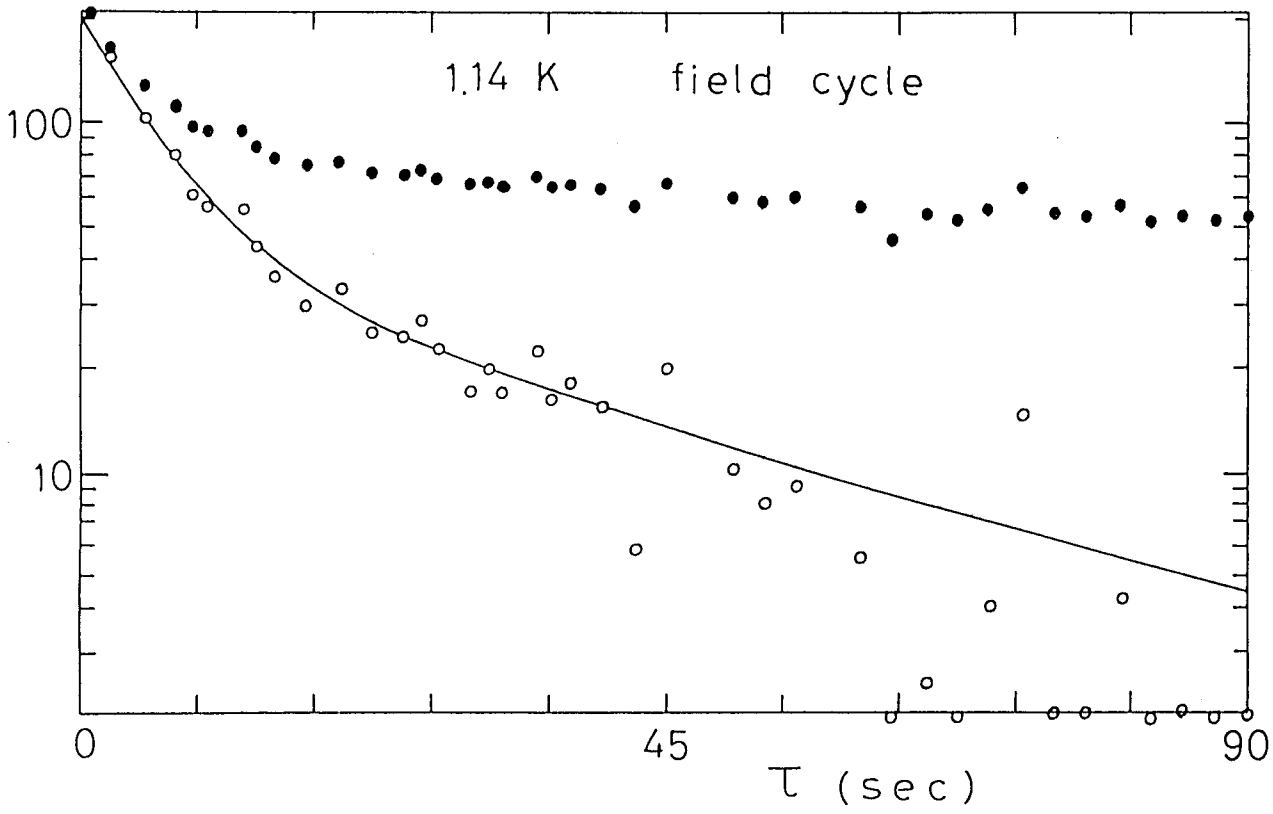

Fig. 19 Best fit curve for the magnetization decay data measured by the field cycle method at 1.14 K.

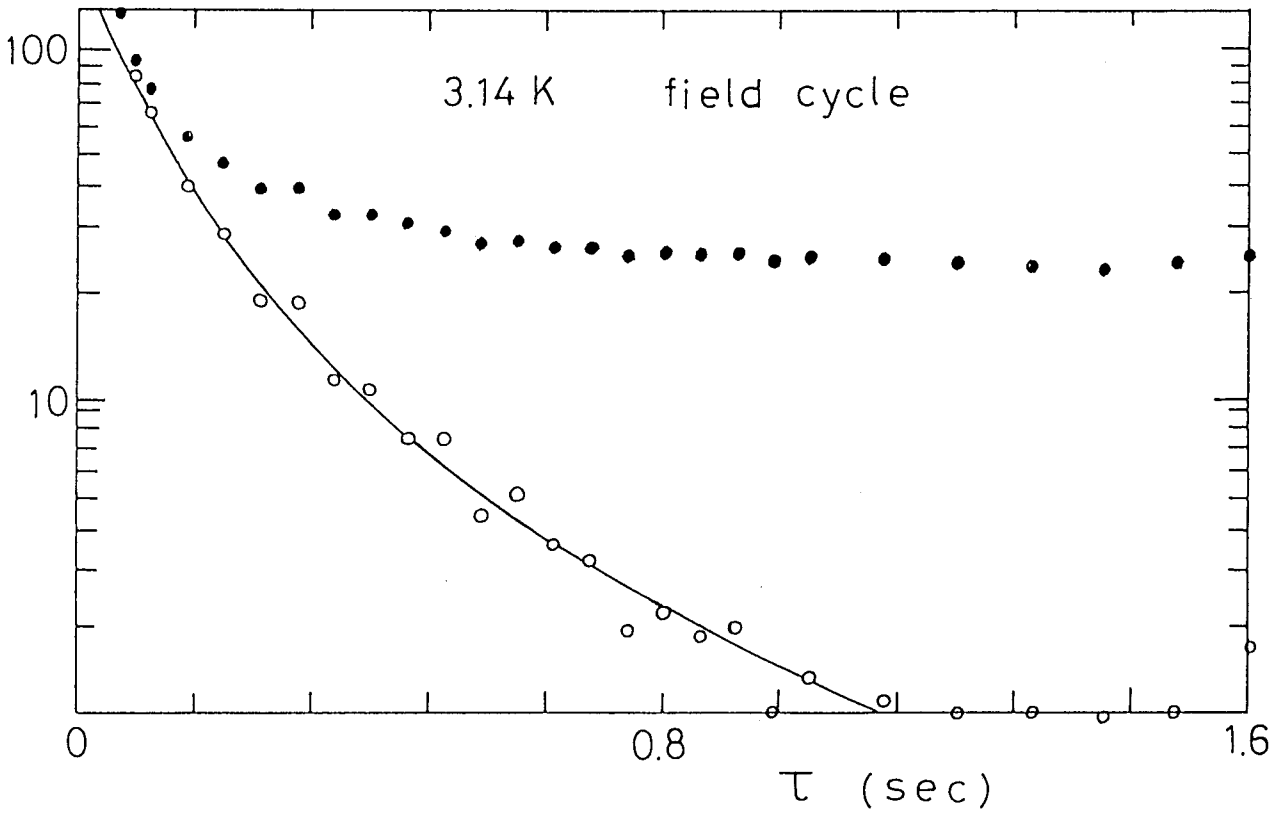

Fig. 20 Best fit curve for the magnetization decay data measured by the field cycle method at 3.14 K.

Table 2 Best fit ratios A:B:C:D in eq. (15) for each temperature.

$T(K)$	A	B	C	D
4.2	8.57×10^{-3}	6.81×10^{-2}	0.477	1
3.75	8.02×10^{-3}	0.108	0.781	1
3.73	1.14×10^{-2}	0.290	1.42	1
3.24	6.00×10^{-3}	0.123	-8.01×10^{-2}	1
3.14	9.00×10^{-3}	0.205	0.459	1
2.73	2.64×10^{-3}	0.149	-0.147	1
2.63	5.00×10^{-3}	0.102	0.142	1
2.53	8.30×10^{-2}	0.248	1.28	1
2.45	4.70×10^{-2}	0.162	1.58	1
2.32	3.50×10^{-2}	0.147	1.21	1
2.19	2.60×10^{-2}	0.487	-1.30×10^{-2}	1
1.98	4.80×10^{-2}	0.724	0.815	1
1.86	2.70×10^{-2}	0.535	2.16	1
1.47	-9.90×10^{-2}	0.626	0.152	1
1.21	-3.90×10^{-2}	0.550	0.380	1
1.14	2.10×10^{-2}	0.305	-0.263	1
0.80	0.150	1.00	0.953	1

5.3 Field Dependence of T_1 in the Field Cycle Method

We should check the probability that the deviation of the measured T_1 from those predicted by the BCS theory originates from the reasons other than the superconducting property. The following case may be considered. In the field cycle method, T_1 is measured in the zero field condition in principle. However, after the external magnetic field is switched off to zero, the flux may be trapped in the superconducting state and some of the ^{51}V nuclei in the flux have the shorter relaxation time. They may make T_1 of the system shoter by spin diffusion.

In order to clear this point we measured the dependence of T_1 on the magnetic field H in which the ^{51}V nuclear spins relax in the field cycle process. The results at 2.77K are shown in Fig. 21. In this figure the value of T_1, 2.8 sec on the vertical axis shows that measured at H=0. T_1 is constant up to 100 Oe, becomes longer with increasing H and is again constant (about 7.6 sec) above 500 Oe.

Hebel-Slichter[6], Anderson-Redfield[16] and Fite-Redfield[17] measured the magnetic field dependence of the spin-lattice relaxation time in metals. Our result is very similar to those obtained by them. According to Anderson-Redfield[16],

$$\frac{T_1}{T_{1K}} = \frac{H^2 + 10\langle(\Delta H)^2\rangle_{AV}/3 + \overline{H_q^2}(1+\overline{\eta^2}/3)}{H^2 + 10\delta\langle(\Delta H)^2\rangle_{AV}/3 + \overline{H_q^2}(3+2\overline{\eta^2}/3)}, \qquad (16)$$

where T_{1K} is the relaxation time when $\langle(\Delta H)^2\rangle_{AV}=0$ and $\overline{H_q^2}=0$, and $\langle(\Delta H)^2\rangle_{AV}$ is the Van Vleck second moment. δ and $\overline{H_q^2}$ are given by the following equations,

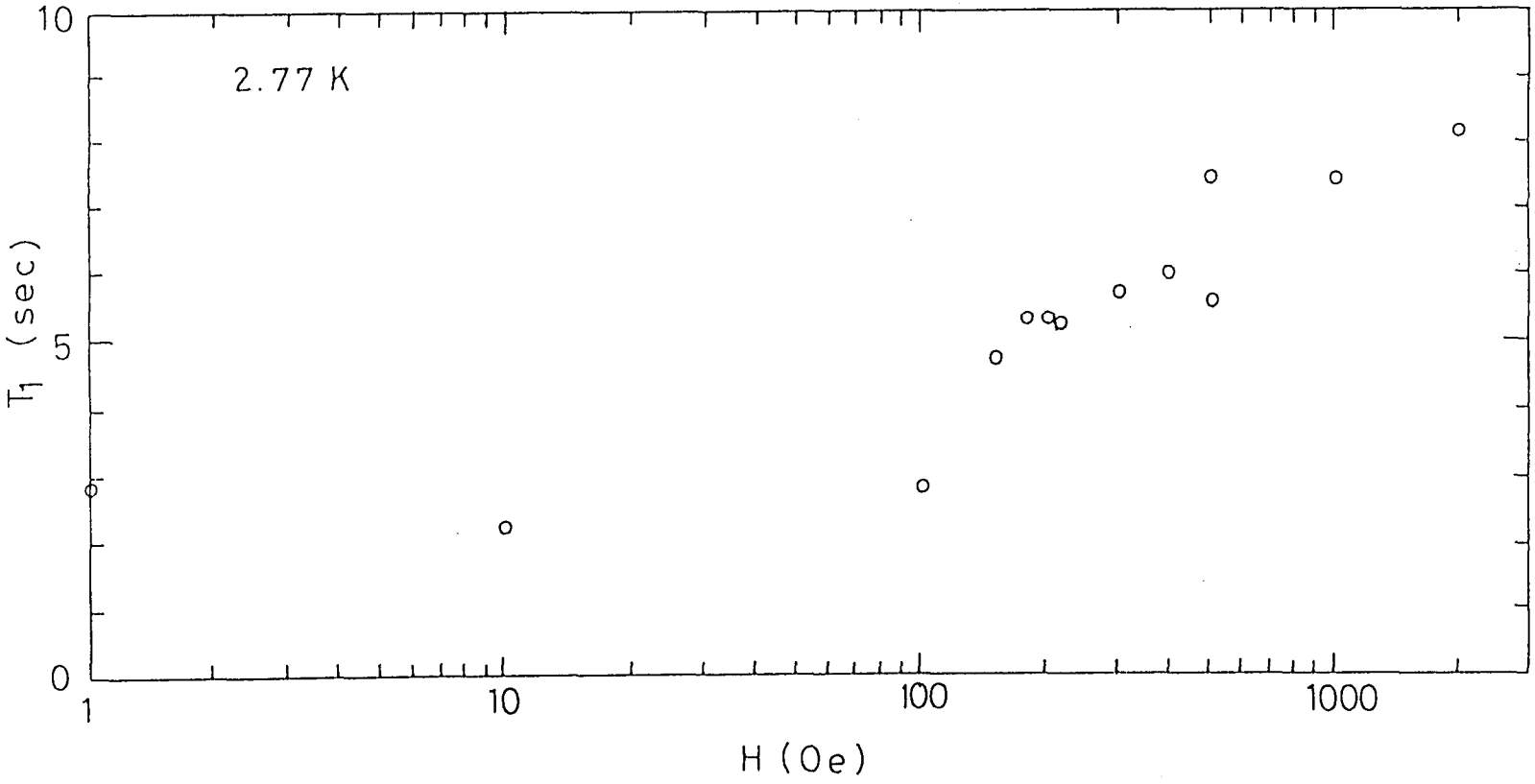

Fig. 21 Field dependence of T_1 measured by the field cycle method at 2.77 K.

$$\delta = 2 + (\Sigma\ K_{jk}\, r_{jk}^{-6}) / \Sigma\, r_{jk}^{-6}, \qquad (17)$$

where r_{jk} is the distance between spins j and k, and K_{jk} expresses the degree of correlation between the fluctuating fields at r_j and r_k due to the conduction electrons, and

$$\overline{H_q^2} = e^4 q^2 Q^2 (4I(I+1)-3)/80(2I-1)^2 I\eta^2\hbar^2, \qquad (18)$$

where $\overline{q^2}$ is the average value of q_i^2, and $\overline{\eta^2}$ is the average value of the quadrupole asymmetry parameter, $q_i^2\eta_i^2/\overline{q^2}$. From the lineshape shown in Fig. 2, H_Q is estimated to be several hundred Oersteds and much larger than $\langle(\Delta H)^2\rangle_{Av}$. Therefore, we get

$$T_1(H=\infty)/T_1(H=0) = (3+2\overline{\eta^2}/3)/(1+\overline{\eta^2}/3). \qquad (19)$$

The measured ratio is about 2.7 and similar to those obtained by Hebel-Slichter[6] and Anderson-Redfield[16], and this value 2.7 is very near to the range from 3.0 to 2.75 if it is supposed $0 \leqq \eta \leqq 1$.

Anyway, from Fig. 21 it can be said that even if the magnetic flux is trapped, it should be less than 100 Oe because T_1 is constant up to 100 Oe. T_1 becomes longer with increasing H, which is against the expectation that T_1 should become shorter with increasing H in the case the spin diffusion mechanism is important. Therefore, the probability that the spin diffusion makes T_1 shorter can be denied in our case. The present values of T_1 measured by the field cycle method are intrinsic. From this

measurement, it is also found that $1/T_1$ measured in zero field is about 2.7 times larger than that measured in high field. Therefore, the difference between the T_1 measured in the constant field and that by the field cycle method is reduced to the factor of 2.4. To explain this difference, we tried to estimate T_1 by fitting eq. (15) with unknown coefficients to the data points measured in the constant field. Two examples of this fitting are shown in Figs. 22 and 23. The result is shown in Fig. 24 by closed circles together with the data measured by the field cycle method (triangles) and those measured in the constant field at 12 MHz and estimated by using eq. (5) (open circles). As shown in this figure the values of $1/T_1$ estimated by eq. (15) (closed circles) are about 2.5 times larger than those by eq. (5) (open circles). Thus the difference stated above is understood reasonably.

In addition to the behavior of $1/T_1$ at low temperature, the enhancement of $1/T_1$ just below T_c reflects the gap anisotropy. If the measured small enhancement of $1/T_1$ just below T_c originates from the depression by the applied external magnetic field of about 10 kOe, our discussion about the energy gap anisotropy will require some change. To investigate this point, we measured the enhancement of $1/T_1$ at 6MHz. The result is shown in Fig. 25, where we estimated T_1 by fitting eq. (5) to the magnetization decay data, and in Fig. 26, where we estimated T_1 by fitting eq. (15) to the data. The deviation of these data from those measured at 12 MHz may be due to the experimental errors. (About this problem of the experimental errors we have a plan to check it in the near future. As discussed above, the $1/T_1$ obtained by fitting

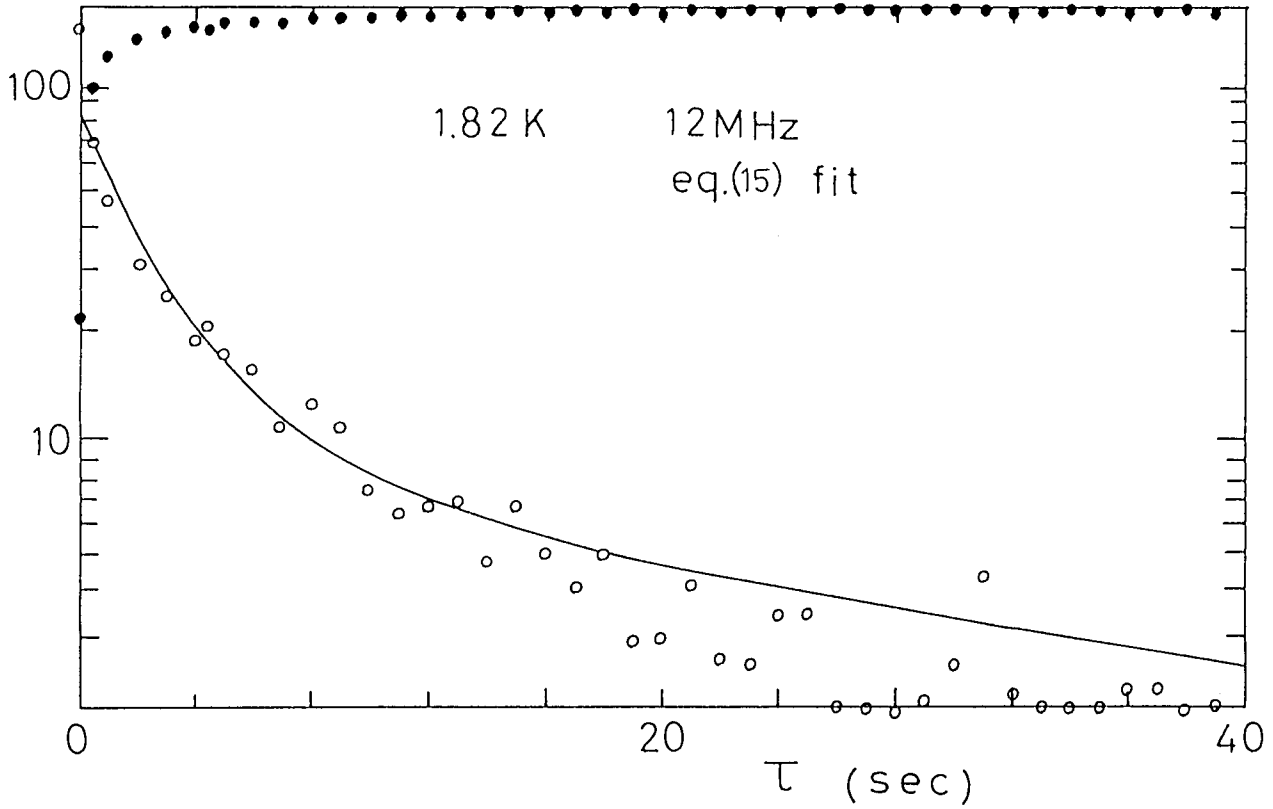

Fig. 22 Best fit curve of eq. (15) to the 12 MHz data at 1.82 K

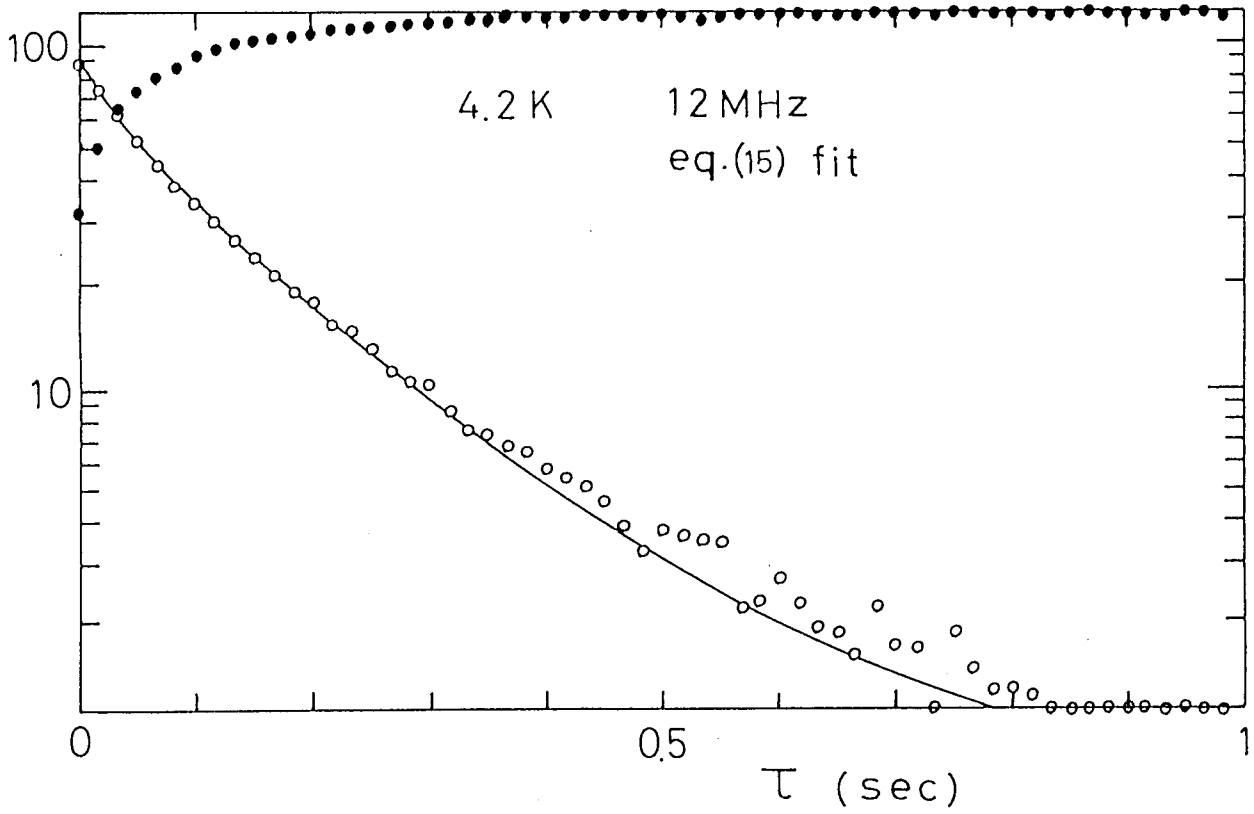

Fig. 23 Best fit curve of eq. (15) to the 12 MHz data at 4.2 K

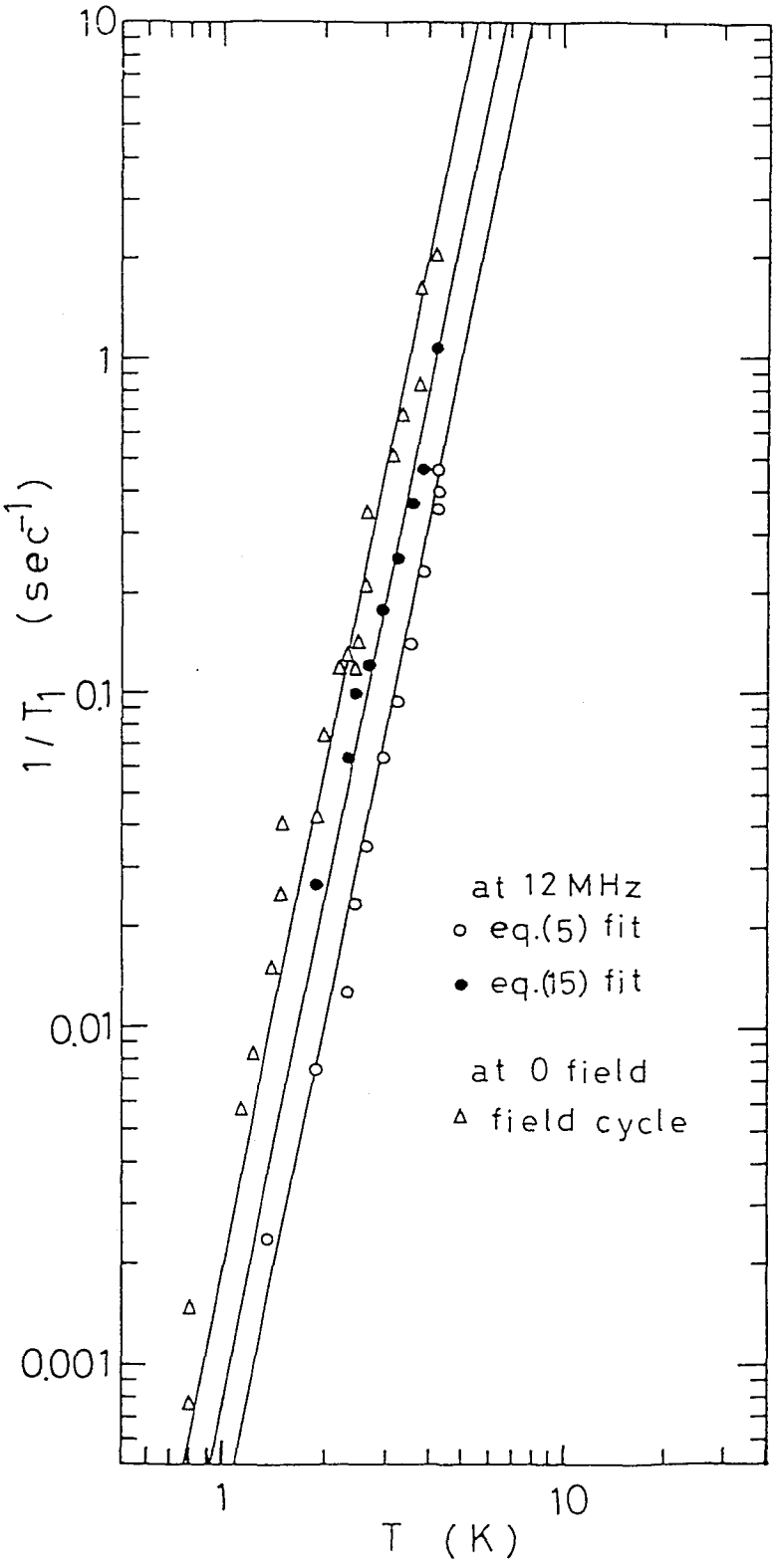

Fig. 24 Comparison of $1/T_1$ estimated by fitting of eq. (5) (open circles), of eq. (15) (closed circles) and those measured by the field cycle method (triangles).

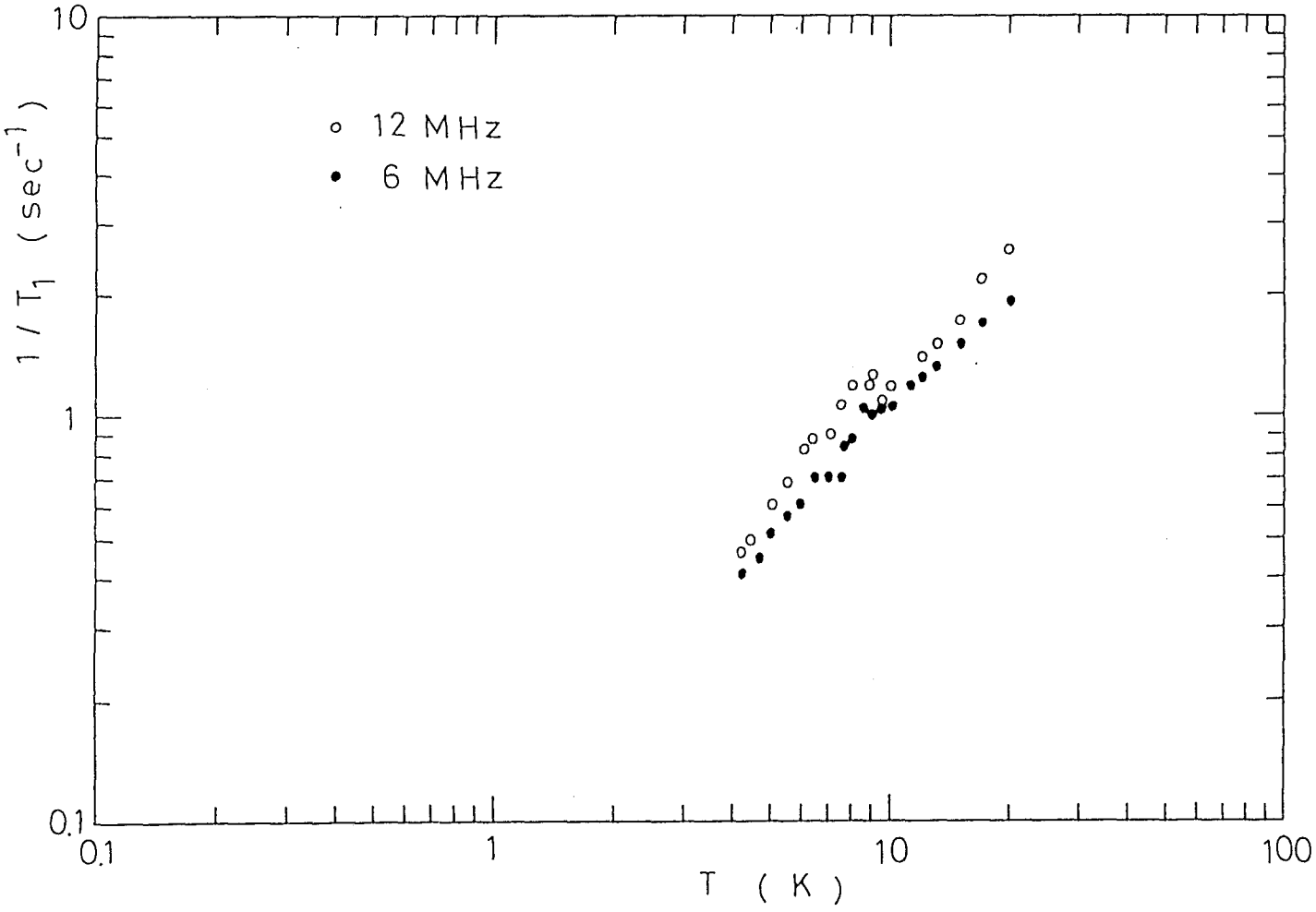

Fig. 25 Comparison of $1/T_1$ estimated by fitting of eq. (5) at 12 MHz (open circles) and 6 MHz (closed circles).

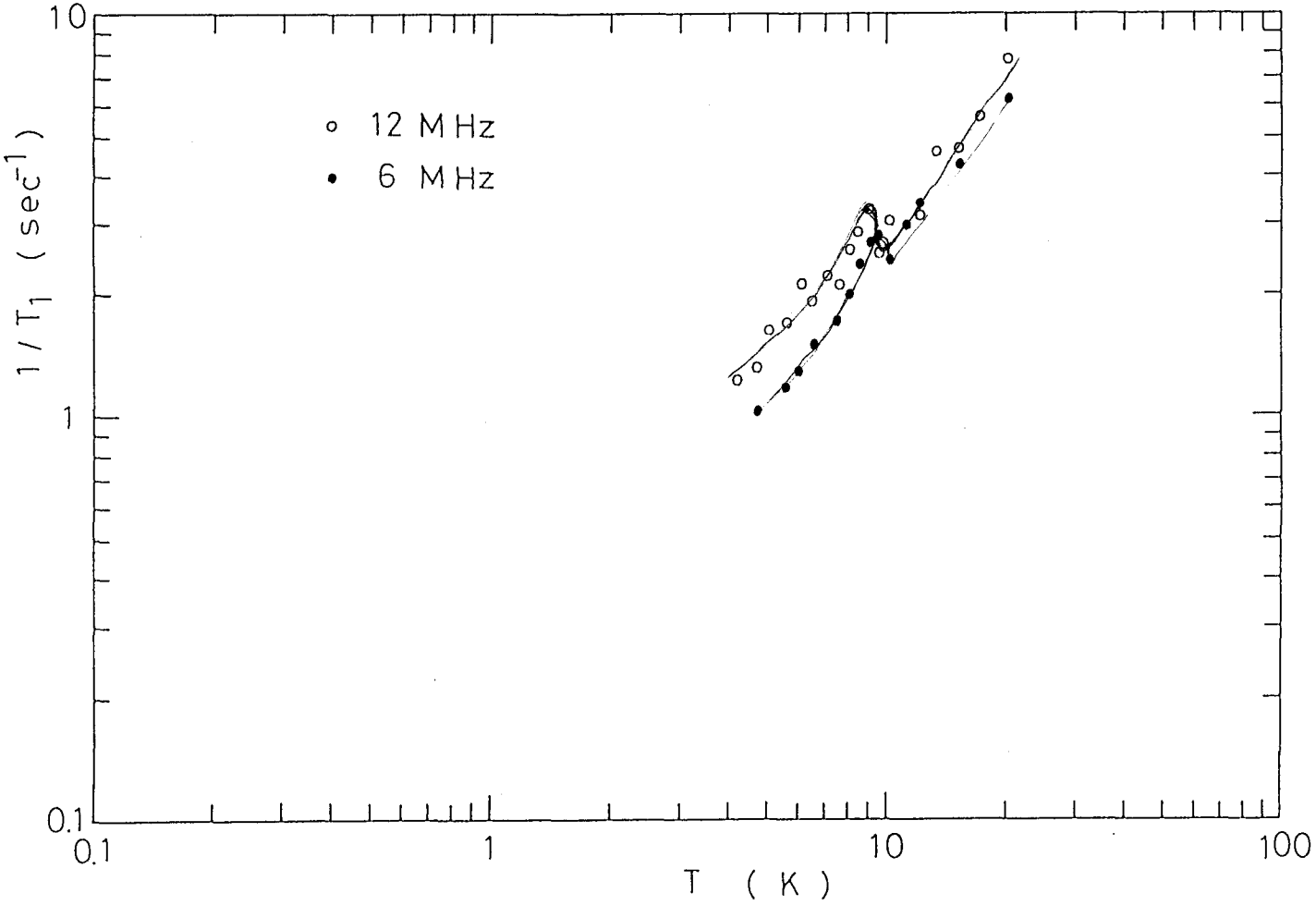

Fig. 26 Comparison of $1/T_1$ estimated by fitting of eq. (15) at 12 MHz (open circles) and 6 MHz (closed circles).

eq. (15) is about 2.5 times as large as that obtained by fitting eq. (5). As shown in Figs. 25 and 26, the depression of the enhancement by the external field does not occur. Masuda et al.[17] pointed out a large field dependence of the enhancement of $1/T_1$ for ^{51}V in V_3Sn. In V_3Sn the enhancement is not observed when measured at 15 MHz, but the ratio of the relaxation time T_{1n}/T_{1s} in the normal and the superconducting state at the peak enhancement temperature is about 2.0 at 5 MHz. If I take into account the difference of T_C and H_{c2} between V_3Sn (T_C=3.6K, H_{c2} = 16 kOe) and HfV_2 (T_C=9.2K, H_{c2} =200 kOe), it appears that the field of 10 kOe for HfV_2 corresponds to a much lower field for V_3Sn. Therefore, it is concluded that the enhancement observed at 12 MHz in HfV_2 is not affected by the applied field.

5.4 Analysis Based on the ABM Model

Now I try to analize our data based on the ABM model and discuss about the density of states $N_S(E)$ which reflects the low energy excitation spectrum at low temperature. The electronic specific heat C_S and the spin-lattice relaxation rate $(1/T_1)_S$ in the superconducting state are expressed by the following equations [10, 18],

$$\frac{C_S}{C_N} = \frac{6}{\pi^2} \cdot \frac{1}{(k_B T)^3} \int_0^\infty \frac{N_S(E)}{N_0} \cdot E^2 \cdot \frac{\exp(E/k_B T)}{(\exp(E/k_B T)+1)^2} dE \quad , \quad (20)$$

and

$$\frac{(T_1)_N}{(T_1)_S} = 2 \int_0^\infty \left[\left(\frac{N_S(E)}{N} \right)^2 + \left(\frac{M_S(E)}{N_0} \right)^2 \right] \cdot \frac{\exp(E/k_B T)}{(\exp(E/k_B T)+1)^2} dE \quad , \quad (21)$$

where C_N and $(1/T_1)_N$ are the specific heat and the relaxation rate in the normal state, respectively, $M_S(E)$ is the coherent factor term, and N_0 the density of states on the Fermi surface in the normal state. Both the measured specific heat and spin-lattice relaxation rate at $T < T_C$ suggest that the superconducting energy gap vanishes at points on the Fermi surface. In this case, $N_S(E)$ is proportional to E^2. [10]

$$N_S(E) = aN_0 \left(\frac{E}{\Delta} \right)^2 \quad , \quad (22)$$

where Δ is the maximum energy gap. The coefficient a should be unity for the ABM state. Substituting eq. (22) into eqs. (20) and (21), I get

$$\frac{C_S}{C_N} = 13.80\, a \cdot \left(\frac{k_B}{\Delta}\right)^2 \cdot T^2 \quad , \tag{23}$$

and

$$\frac{(T_1)_N}{(T_1)_S} = 72.64\, a^2 \cdot \left(\frac{k_B}{\Delta}\right)^4 \cdot T^4 \quad . \tag{24}$$

From eq. (23) and the present specific heat data shown in Fig. 1 (b), a is estimated to be 0.60 if we use the best fit gap parameter $\Delta / k_B T_C$ = 2.014X0.8 for the present T_1 data discussed above. Using the same gap parameter and the T_1 data we can also estimate a to be 1.24 from eq. (24) by extrapolating $T_1 T$ = 8.47 sec · K measured between 9.4K and 20K to the superconducting state. Both of the above obtained values 0.60 and 1.24 are not so far from unity expected for the case the energy gap vanishes at two points on the Fermi surface by the ABM model.

§6. Conclusion

In the strong electron-phonon coupling superconductor HfV_2, the anisotropy of the superconducting energy gap was found by the ^{51}V NMR T_1 and the specific heat measurements. At low temperatures, the electronic part of the specific heat and the nuclear relaxation rate $1/T_1$ obey the T^3 and T^5 law, respectively. These facts are inconsistent with the $\exp(-\Delta/k_B T)$ law predicted by the BCS theory and indicate that the superconducting energy gap is anisotropic and vanishes at points on the Fermi surface. Actually, the agreement between the $1/T_1$ data and the calculated curve based on the ABM gap model with the gap parameter $\Delta/k_B T_C = 2.014 \times 0.8$ is satisfactorily good at low temperatures.

It was also found that the frequency dependence of $1/T_1$ is weak and the small enhancement just below T_C is not affected by the external field at 12 MHz. The same T^5 dependence of $1/T_1$ well below T_C was also certified by the field cycle method. The dependence of T_1 on the magnetic field in which the ^{51}V nuclear spins relax in the field cycle process measured at 2.77 K can be explained by the electric quadrupole effect.

In the normal state, $1/T_1 T$ is constant between 9.4 K and 20 K, decreases with increasing temperature and is nearly constant at $T > 130$ K. This temperature dependence of $1/T_1 T$ between 20 K and 100 K can be explained by using the narrow band models with the half width of about 100 K.

The formation of the narrow band and the energy gap anisotropy support the concept of the TLS model that they are originated from the same correlation among electrons as in the heavy Fermion.

Acknowledgments

The author would like to express his sincere thanks to Professor K. Asayama for his continuous guidance, discussions, and encouragement throughout the course of this work.

He wishes to express his appreciation to Professor Y. Kitaoka for his concern and guidance as an adviser of this work.

He would like to thank Professor T. Kanashiro for his continuous encouragement, valuable discussions and the careful reading of the manuscript. He is also much indebted to Professor T. Taki and Professor Y. Michihiro for their many valuable discussions and aids.

Special thanks are due to Professor T. Ohno, who has befriended me innumerable times, and has been very helpful in many ways for the fulfilment of this work.

The author thanks Professor K. Amaya for the specific heat measurement.

Thanks are also due to the cooperation of the colleagues at Asayama laboratory.

References

1) M. Weger and I. B. Goldberg: Solid State Physics, ed. H. Ehrenreich, F. Seitz and D. Turnbull (Academic Press, New York and London, 1973) Vol. 28, p. 1.

S. V. Vonsovsky, Yu. A. Izyumov and E. Z. Kurmaev: Superconductivity of Transition Metals (Springer-Verlag, Berlin, Heidelberg, New York, 1982) p. 259

L. R. Testardi: Rev. Mod. Phys., 47 (1975) 637

2) P. W. Anderson and C. C. Yu: in Highlights of Condensed Matter Theory ed. F. Bassani, F. Fomi and M. P. Tosi (North-Holland, Amsterdam, 1985) p. 767.

C. C. Yu and P. W. Anderson: Phys. Rev. B29 (1984) 6165.

3) K. Vladar and A. Zawadowski: Phys. Rev. B28 (1983) 1564; B28 (1983) 1582; B28 (1983) 1596.

4) T. Matsuura and K. Miyake: J. Phys. Soc. Jpn. 55 (1986) 29; 55 (1986) 610.

5) K. Miyake, T. Matsuura and C. M. Varma: Solid State Commun. 71 (1989) 1149.

6) L. C. Hebel and C. P. Slichter: Phys. Rev. 113 (1959) 1504.

7) B. Luthi, M. Herrman, W. Assmus, H. Schmidt, H. Rietschel, H. Wuhl, V. Gottwick, G. Sparn and F. Steglich: Z. Phys. B60 (1985) 387.

8) F. Steglich, J. Aarts, C. D. Bredl, W. Lieke, D. Mescheded, W. Franz and H. Schafer: Phys. Rev. Lett. 43 (1979) 1892.

9) W. L. McMillan : Phys. Rev. 167 (1968) 331.

10) P. W. Anderson and P. Morel: Phys. Rev. 123 (1961) 1911.

11) A. Narath: Phys. Rev. 162 (1961) 320.

12) J. W. Hafstrom, G. S. Knapp and A. T. Aldred: Phys. Rev. B17 (1978)

2892.

13) B. G. Silbernagel and M. Weger: Phys. Rev. Lett. 17 (1966) 384.

14) K. Asayama and Y. Masuda: J. Phys. Soc. Jpn. 26 (1969) 206.

15) Y. Masuda and A. G. Redfield: Phys. Rev. 125 (1962) 159.

16) A. G. Anderson and A. G. Redfield: Phys. Rev. 116 (1959) 583.

17) Y. Masuda and N. Okubo: J. Phys. Soc. Jpn., 26 (1969) 309.

18) D. E. Maclaughlin: Solid State Physics, ed. H. Ehrenreich, F. Seitz and D. Turnbull (Academic Press, New York and London, 1973) Vol. 32 (1976) p. 1.